Chapter 7

RECRYSTALLIZATION OF SINGLE-PHASE ALLOYS

7.1 INTRODUCTION

Recovery, which was discussed in the last chapter, is a relatively homogeneous process in terms of both space and time. When viewed on a scale which is larger than the cell or subgrain size, most areas of a sample are changing in a similar way. Recovery progresses gradually with time and there is no readily identifiable beginning or end of the process. In contrast, recrystallization involves the formation of new strain-free grains in certain parts of the specimen and the subsequent growth of these to consume the deformed or recovered microstructure (fig. 1.1c,d). The microstructure at any time is divided into recrystallized or non-recrystallized regions as shown in figure 7.1, and the fraction recrystallized increases from 0 to 1 as the transformation proceeds, as shown in the in-situ annealing sequence of figure 7.2. This is typical of a **discontinuous** annealing phenomenon as defined in §1.1.

Recrystallization of the deformed microstructure is often called **primary recrystallization** in order to distinguish it from the process of **abnormal grain growth** which may occur in fully recrystallized material and which is sometimes called **secondary recrystallization** (§11.5). We will always use the unqualified term **recrystallization** to mean primary recrystallization.

It is convenient to divide primary recrystallization into two regimes, **nucleation** which corresponds to the first appearance of new grains in the microstructure and **growth**
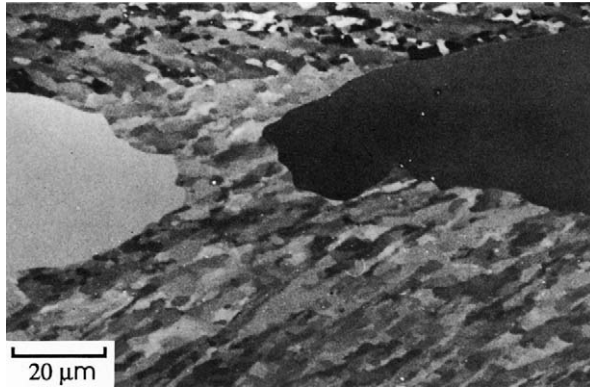
Fig. 7.1.   An SEM channelling contrast micrograph of aluminium showing recrystallized grains growing into the recovered subgrain structure.

during which the new grains replace deformed material. Although these two events occur consecutively for any particular grain, both nucleation and growth may be occurring at any time throughout the specimen. The kinetics of recrystallization are therefore superficially similar to those of a phase transformation which occurs by nucleation and growth. In discussing the origin of recrystallization, the term **'nucleation'** which is conventionally used, is not appropriate because, as will be further discussed in §7.6.1, nucleation in the classic thermodynamic sense does not occur. A more accurate description of the process would be **'initiation',** although, for simplicity, we will use the accepted terminology.

The progress of recrystallization with time during isothermal annealing is commonly represented by a plot of the **volume fraction of material recrystallized (X_V)** as a function of **log(time).** This plot usually has the characteristic sigmoidal form of figure 7.3 and typically shows an apparent incubation time before recrystallization is detected. This is followed by an increasing rate of recrystallization, a linear region, and finally a decreasing rate of recrystallization.

In this chapter we will consider the origin of recrystallization, and general aspects such as the kinetics and other factors which affect both the process of recrystallization and the final microstructure. We will mainly be concerned with the behaviour of single-phase alloys, as the recrystallization of two-phase alloys is considered separately in chapter 9. The mobility and migration of the grain boundaries during recrystallization is considered in more detail in chapter 5, and the orientation of the recrystallized grains (the recrystallization texture), is discussed in chapter 12.

It has recently become apparent that the recrystallization of metals after very large strain deformation may be quite different from that after low or moderate strains, and that the discontinuous recrystallization which is the subject of this chapter, is replaced by a process of **continuous recrystallization.** This topic is the subject of chapter 14.
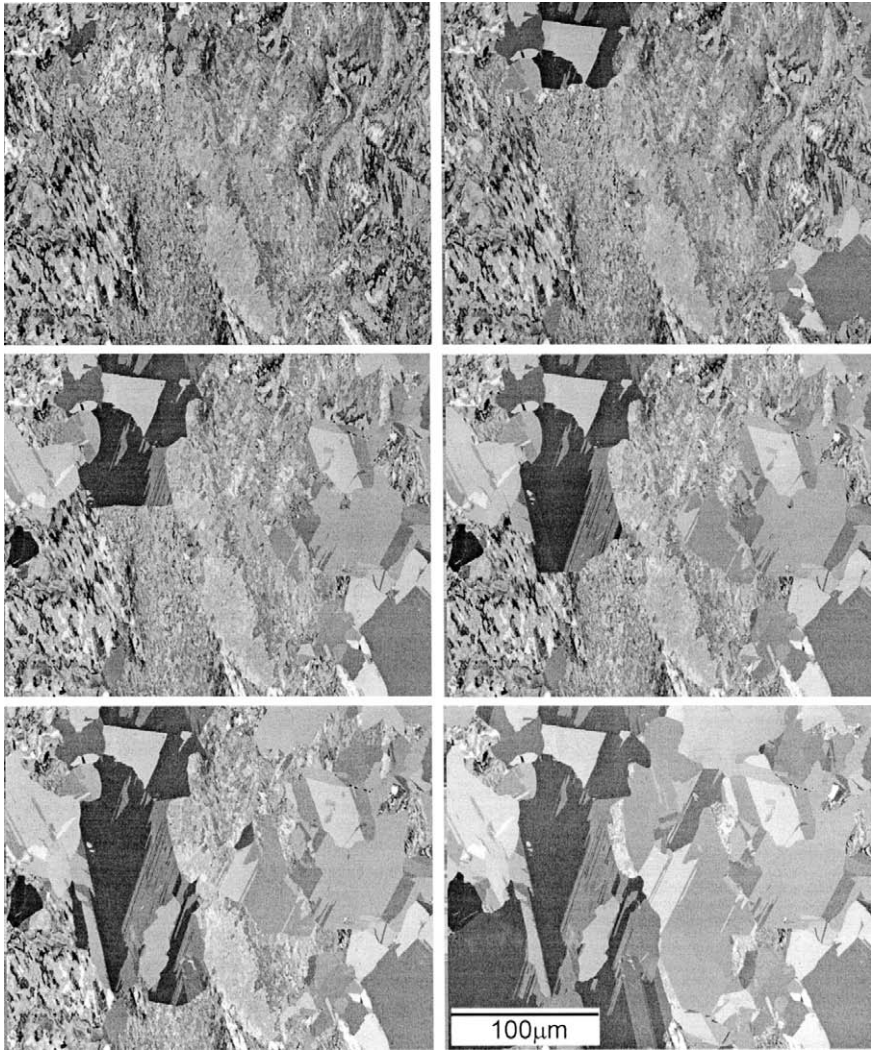
Fig. 7.2. Recrystallization of deformed copper observed during in-situ annealing in the SEM. Video sequences of this and other in-situ annealing experiments can be viewed at **www.recrystallization.info.**

7.1.1 Quantifying recrystallization

Recrystallization is a microstructural transformation, which is most directly measured by quantitative metallography (appendix 2). However, it is also possible to follow the progress of recrystallization by the measurement of various physical or mechanical properties.
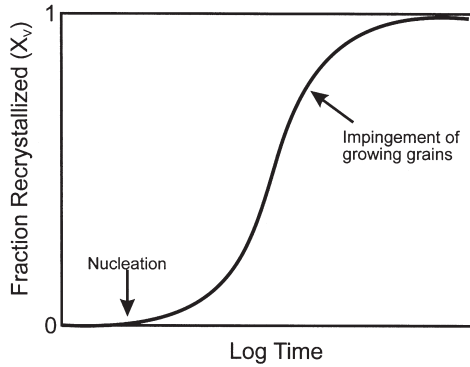
Fig. 7.3.   Typical recrystallization kinetics during isothermal annealing.

7.1.1.1 The overall transformation

The extent of recrystallization is often described by X_V, and for isothermal experiments it is convenient to use the time at which recrystallization is 50% complete $(t_{0.5})$, as a measure of the rate of recrystallization. For isochronal experiments, where annealing is carried out at various temperatures for a constant time, e.g. 1 hr, then the **recrystallization temperature,** is usually defined as the temperature at which the material is 50% recrystallized.

Although such measurements of the recrystallization process have practical value, more fundamental measurements of recrystallization are obtained by separate reference to the constituent **nucleation and growth processes.**

7.1.1.2 Nucleation

Our first difficulty lies in defining what we mean by a **recrystallization nucleus.** A working definition might be **a crystallite of low internal energy growing into deformed or recovered material from which it is separated by a high angle grain boundary.**

If the number of nuclei per unit volume **(N)** remains constant during recrystallization, then this is the key parameter. However, if this is not the case, the **nucleation rate** $\dot{N} = dN/dt$ also needs to be considered. As nucleation of recrystallization is a very complex process, the nucleation rate is not expected to be a simple parameter. Early work indicated that the rate was not always constant during recrystallization as shown in figure 7.4.

However, such measurements need to be regarded with caution, particularly at the early stages of recrystallization, because the number of nuclei observed depends strongly on the technique used to detect them. For example in figure 7.4a are there really no nuclei present at times shorter than 1000 sec or were they just too small to be detected by optical microscopy? Is the initial rising nucleation rate shown in figure 7.4b a real effect or does it reflect the difficulty of detecting small nuclei, in which case perhaps this figure really represents a monotonically decreasing nucleation rate?
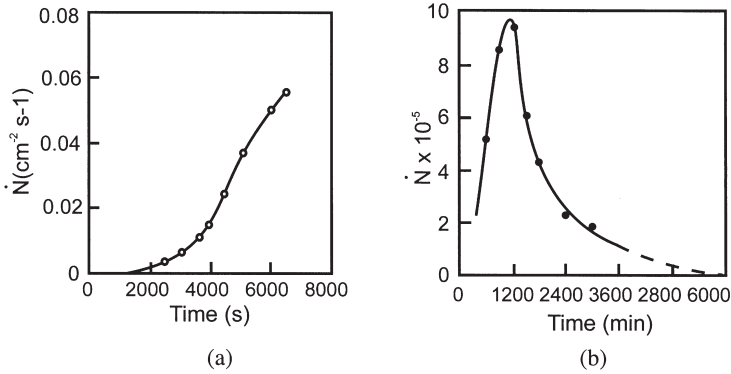
Fig. 7.4.   The variation of nucleation rate $(\dot{N})$ with time during the annealing of 5% deformed aluminium, annealed at 350°C. (a) Initial grain size 45 μm, (b) initial grain size 130 μm, (Anderson and Mehl 1945).

We must recognise that although formal models of the recrystallization kinetics (§7.3) usually refer to nucleation rates, these are often very difficult to measure experimentally. When we come to consider the mechanisms and sites of nucleation (§7.6), it will be clear that in most cases, it is not yet possible to obtain a realistic quantitative model for the number of nuclei and its variation with time and other parameters.

7.1.1.3 Growth

The growth of the new grains during recrystallization is more readily analysed than is their nucleation. It is generally accepted (§5.1.3) that the velocity $(\mathbf{v})$ of a high angle grain boundary, which is also the growth rate $(\dot{\mathbf{G}})$ is given by

$$\mathbf{v} = \dot{\mathbf{G}} = MP \qquad (7.1)$$

where M is the boundary mobility and P is the net pressure on the boundary (§5.1.3).

Driving pressure – The driving pressure (P_d) for recrystallization is provided by the dislocation density (ρ), which results in a stored energy (E_D) given by equation 2.6. The resultant driving force for recrystallization is then given approximately as:

$$P_d = E_D = \alpha \rho G \, b^2 \qquad (7.2)$$

where α is a constant of the order of 0.5.

For a dislocation density of 10^{15} m^{-2}, typical of a metal, and taking Gb^2 as 10^{-9} N, the driving pressure for primary recrystallization is of the order of 1MPa. If the dislocations are in the form of low angle boundaries, then, using equation 2.8, the driving pressure may be expressed in terms of subgrain size and misorientation.

Boundary curvature – If we consider a small, spherical, new grain of radius R, growing into the deformed structure, there is an opposing force which comes from the curvature of a high angle grain boundary of specific energy γ_b. The grain boundary area will be reduced and the energy lowered if the grain were to shrink, and there is thus a retarding pressure on the boundary given by the Gibbs-Thomson relationship:

$$P_c = \frac{2\gamma_b}{R} \tag{7.3}$$

This pressure is however only significant in the early stages of recrystallization when the new grains are small. For a grain boundary energy of 0.5 Jm^{-2} and the driving force discussed above, we find that P_c is equal to P_d when R is ~1 μm. Below this grain size there would therefore be no net driving force for recrystallization. During the recrystallization of alloys, other retarding forces arising from solutes or second-phase particles may be important, and these will be discussed elsewhere.

The pressure on a grain boundary and therefore the boundary velocity, may not remain constant during recrystallization. In particular, as will be discussed later, the driving force may be lowered by concurrent recovery and both the driving force and the boundary mobility may vary through the specimen. Therefore the growth rate (**Ġ**), which is an important parameter in any model of recrystallization is also a complex function of the material and the deformation and annealing conditions.

7.1.2 The laws of recrystallization

In this chapter we are primarily concerned with the principles of recrystallization, and although we will refer to selected work from the literature, no attempt will be made to present a detailed survey of the numerous experimental investigations which have been carried out over the past 50 years. Cotterill and Mould (1976) provide an extensive bibliography of the earlier work on a wide variety of materials.

In order to introduce the subject, it is of interest to recall one of the earliest attempts to rationalise the recrystallization behaviour of materials, viz the formulation of the so-called **laws of recrystallization** (Mehl 1948, Burke and Turnbull 1952). This series of qualitative statements, based on the results of a large body of experimental work, predicts the effects of the initial microstructure (grain size), and processing parameters (deformation strain and annealing temperature), on the time for recrystallization and on the grain size after recrystallization. These rules are obeyed in most cases and are easily rationalised if recrystallization is considered to be a nucleation and growth phenomenon, controlled by thermally activated processes, whose driving force is provided by the stored energy of deformation.

(i)   **A minimum deformation is needed to initiate recrystallization.** The deformation must be sufficient to provide a nucleus for the recrystallization and to provide the necessary driving force to sustain its growth.

(ii) **The temperature at which recrystallization occurs decreases as the time of anneal increases.** This follows from the fact that the microscopic mechanisms controlling

recrystallization are thermally activated and the relationship between the recrystallization rate and the temperature is given by the Arrhenius equation.

(iii) **The temperature at which recrystallization occurs decreases as strain increases.** The stored energy, which provides the driving force for recrystallization, increases with strain. Both nucleation and growth are therefore more rapid or occur at a lower temperature in a more highly deformed material.

(iv) **The recrystallized grain size depends primarily on the amount of deformation, being smaller for large amounts of deformation.** The number of nuclei or the nucleation rate are more affected by strain than the growth rate. Therefore a higher strain will provide more nuclei per unit volume and hence a smaller final grain size.

(v) **For a given amount of deformation the recrystallization temperature will be increased by:**

   A larger starting grain size. Grain boundaries are favoured sites for nucleation, therefore a large initial grain size provides fewer nucleation sites, the nucleation rate is lowered, and recrystallization is slower or occurs at higher temperatures.

   A higher deformation temperature. At higher temperatures of deformation, more recovery occurs during the deformation (dynamic recovery), and the stored energy is thus lower than for a similar strain at a lower deformation temperature.

7.2 FACTORS AFFECTING THE RATE OF RECRYSTALLIZATION

When Burke and Turnbull (1952) reviewed the subject, they were able to rationalise a large body of experimental data into the comparatively simple concepts embodied in the above 'laws of recrystallization'. However, later research has shown that recrystallization is a much more complex process than was envisaged at that time, and in addition, we now know that it is difficult to extrapolate some of the earlier work, much of which was carried out on materials of high purity deformed to low strains by uniaxial deformation, to industrial alloys deformed to large strains. Although the laws of recrystallization still provide a very useful guide to the overall behaviour, we now recognise there are so many other important material and processing parameters that need to be taken into account that any attempt to understand recrystallization needs to address the phenomena at a much finer microstructural level than was possible 50 years ago.

In the following section, we will consider some of the important factors which are known to affect the rate at which recrystallization occurs in materials.

7.2.1 The deformed structure

7.2.1.1 The amount of strain
The amount, and to some extent the type of deformation, affect the rate of recrystallization, because the deformation alters the amount of stored energy and the
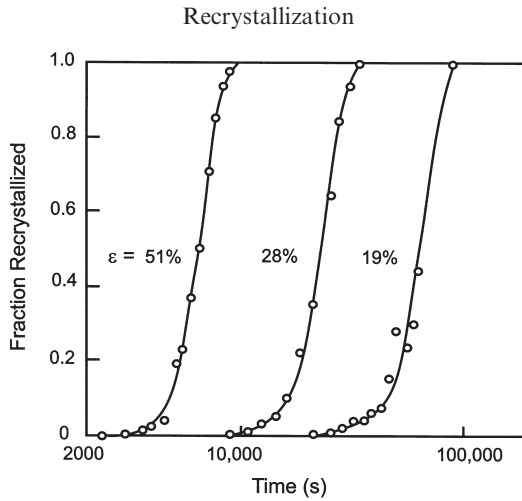
Fig. 7.5.   The effect of tensile strain on the recrystallization kinetics of aluminium annealed at 350°C, (Anderson and Mehl 1945).

number of effective nuclei. As will be discussed in §7.6, the type of nucleation site may also be a function of strain. There is a minimum amount of strain, typically 1–3%, below which recrystallization will not occur. Above this strain the rate of recrystalliza-tion increases, levelling out to a maximum value at true strains of ~2–4. The effect of tensile strain on the recrystallization kinetics of aluminium is shown in figure 7.5.

7.2.1.2 The mode of deformation

The mode of deformation also affects the recrystallization rate. Single crystals deformed in single glide, recover on annealing, but may not recrystallize, because the dislocation structure (similar to that shown in fig. 6.7) does not contain the heterogeneities and orientation gradients needed to provide a nucleation site. The best examples of this effect are found in the hexagonal metals which deform by glide on the basal plane. For example Haase and Schmid (1925) showed that even after extensive plastic strain, crystals of zinc would recover their initial properties completely without recrystalliza-tion. At the other extreme, a metal which has undergone a deformation resulting in little or no overall shape change (i.e. most of the deformation is **redundant**) may nevertheless recrystallize readily. The effect of the deformation mode on recrystallization is complex. For example in both iron (Michalak and Hibbard 1957) and copper (Michalak and Hibbard 1961) it was found that straight rolling induces more rapid recrystallization than does cross rolling to the same reduction in thickness. Barto and Ebert (1971) deformed molybdenum to a true strain of 0.3 by tension, wire drawing, rolling and compression and found that the subsequent recrystallization rate was highest for the tensile deformed material and decreased in the above order for the other samples.

7.2.1.3 Strain path changes

In many metal working operations, the **strain path** is not constant, and may even be reversed. An example of this is in rolling, where shear deformation near the surface
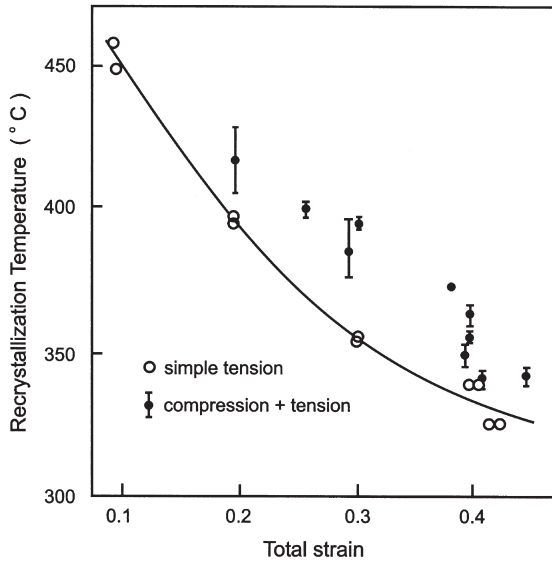
Fig. 7.6.   The recrystallization temperature of copper as a function of the total applied strain in specimens deformed by tension or by a combination of tension and compression, (Lindh et al. 1993).

changes sign. Although the prime interest in strain path effects is their effect on formability, there is also interest in determining how such strain path effects influence the subsequent recrystallization behaviour.

Experiments to determine the role of strain path on the recrystallization of high purity copper have been reported by Lindh et al. (1993). They carried out tension and combined tension and compression experiments and measured the recrystallization temperature. For specimens deformed solely by tension, the recrystallization temperature decreased with increasing tensile strain (fig. 7.6) as would be expected. However, specimens deformed to the same **total permanent strain** (ε_{perm}) by tension and compression were found to recrystallize at higher temperatures. By reading across from the data points for the tension/compression samples to the curve for the tensile specimens of figure 7.6, an equivalent **recrystallization strain** (ε_{equ}^{R}) could be determined for the tensile/compression samples, and this was given by

$$\varepsilon_{equ}^{R} = \varepsilon_{perm} + \eta\varepsilon_{red} \tag{7.4}$$

where ε_{red} is the redundant strain and η a constant found to be 0.65. This shows that the redundant strain is only 0.65 times as effective in promoting recrystallization as is the permanent strain.

Embury et al. (1992) compared the recrystallization behaviour of cubes of pure aluminium deformed in uniaxial compression with similar specimens which were
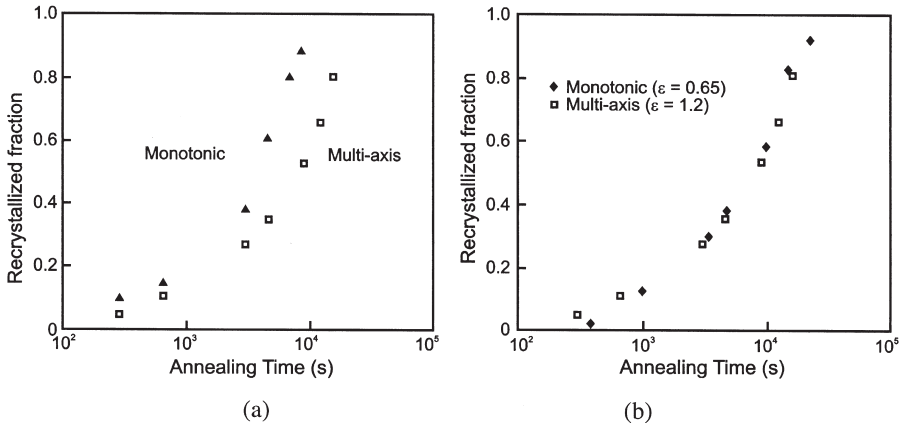
Fig. 7.7. The effect of redundant deformation on the recrystallization of pure aluminium. The recrystallization kinetics for specimens deformed monotonically are compared with those of specimens deformed by multi-axis compression. (a) Specimens deformed to the same equivalent strain (0.7), (b) specimens deformed to the same equivalent stress, (Embury et al. 1992).

deformed incrementally in different directions so as to produce no overall shape change. Their results (fig. 7.7a) show that for the same equivalent strain the specimens deformed by multi-axis compression recrystallized more slowly than the specimens deformed by monotonic compression, in agreement with the results of figure 7.6. However, if the specimens were deformed to the same level of **stress,** as shown in figure 7.7b, the recrystallization kinetics of the specimens were similar.

Zhu and Sellars (1997) investigated the effect of reversed uniaxial deformation on aluminium. They found similar effects on the recrystallization kinetics to those cited above, and also showed that the recrystallized grain size was much larger for a given total strain if the strain path involved tension and compression. They also investigated the effects of strain path change on the deformation microstructure, and found a lower dislocation density after strain reversal.

A simple interpretation of all these results is that the dislocation density and hence the flow stress are reduced on strain reversal. The lower driving pressure for recrystallization resulting in slower recrystallization and larger recrystallized grain sizes. However, a detailed explanation of the effect of deformation mode on recrystallization cannot be given, until the effects of redundant deformation on the microstructure are adequately understood.

A remarkable example of how a highly deformed microstructure can be 'undeformed' is found in the work of Farag et al. (1968). These authors found that the elongated grain structure produced in pure aluminium by a strain in torsion of 2.3 at 400°C could be returned to an equiaxed grain structure if an equal and opposite strain was subsequently given.

7.2.2 The grain orientations

7.2.2.1 Single crystals

As discussed in chapter 2, the microstructure and stored energy of a deformed grain depends strongly on the active slip systems and hence on its orientation. Therefore the initial orientation as well as the 'orientation path' during deformation, will affect both the nucleation sites and the driving force for recrystallization.

Hibbard and Tully (1961) measured the recrystallization kinetics of both copper and silicon-iron single crystals of various orientations, which had been cold rolled 80%, and found significant differences in rates of recrystallization as shown for silicon-iron in table 7.1.

Brown and Hatherly (1970) investigated the effect of orientation on the recrystallization kinetics of copper single crystals which had been rolled to a reduction of 98.6%. The recrystallization times on annealing at 300°C varied between 5 and 1000 min. These compared with a recrystallization time of 1 minute for a polycrystalline specimen deformed to the same strain. It was found, in agreement with the first two samples in table 7.1, that the recrystallization kinetics could not be clearly associated with the texture resulting from deformation. For example, both {110}<112> and {110}<001> crystals developed similar {110}<112> rolling textures, but due to the differences in the nature of the deformed structure, the former recrystallized 50 times more slowly. Differences between the recrystallization kinetics and textures of the single crystals and the reference polycrystal in the above investigation, serve to highlight the importance of grain boundaries during recrystallization and show that care must be taken in using data from single crystal experiments to predict the behaviour of polycrystals.

The recent development of techniques such as EBSD which enable detailed characterisation of local orientations (appendix 2.1.4), has helped to clarify many issues concerning the recrystallization of single crystals, into which there has been considerable recent research (e.g. Driver 1995, Mohamed and Bacroix 2000, Driver et al. 2000, Godfrey et al. 2001). The general conclusions are in agreement with the earlier researches and show that the stored energy after deformation is strongly dependent on crystal orientation, and that this has a marked influence on the rate of recrystallization.

Table 7.1
Recrystallization of silicon–iron single crystals at 600°C (Hibbard and Tulley 1961).

Initial orientation	Final orientation	Time for 50% recrystallization (s)	Orientation after recrystallization
{111}<112>	{111}<112>	200	{110}<001>
{110}<001>	{111}<112>	1000	{110}<001>
{100}<001>	{001}<210>	7000	{001}<210>
{100}<011>	{100}<011>	No recrystallization	{100}<011>

7.2.2.2 Polycrystals

In polycrystalline materials there is evidence that the overall recrystallization rate may be dependent on both the starting texture and the final deformation texture. In iron, the orientation dependence of the stored energy after deformation has been determined (§2.2.3), and it has been predicted on this basis that the various texture components will recrystallize in the sequence shown in figure 7.8. Recent work (Hutchinson and Ryde 1995) has confirmed the trends shown in this figure. In aluminium alloys, Blade and Morris (1975) have shown that differences in the texture formed after hot rolling and annealing lead to differences in recrystallization kinetics when the material is subsequently cold rolled and annealed.

The observations of inhomogeneous recrystallization discussed in §7.4 provide further evidence of the variation of recrystallization rate for different components of the deformation texture.

7.2.2.3 The effect of boundary character on growth rate

The orientation relationships between deformed and recrystallizing grains may also have a strong effect on the growth rate during recrystallization. This is a consequence of the dependence of grain boundary mobility **(M)** on boundary character discussed in chapter 5, and it may be seen from equation 7.1, that this directly influences the growth rate.

Grain boundaries of high mobility will not only cause more rapid recrystallization, but may strongly influence the recrystallization texture. This effect, which is known as **oriented growth,** is discussed in detail in §12.3.2. It has been pointed out by Juul Jensen (1995b) that oriented growth effects may also result from low angle boundaries of low mobility, if recrystallizing grains encounter deformed regions of a similar orientation.

The important general conclusions to be drawn from this section are:

- **Recrystallization of different texture components** will occur at different rates, and will inevitably lead to inhomogeneous recrystallization (§7.4).
- **The strain path history** affects both the stored energy and the heterogeneities of the microstructure, and therefore apparently identical texture components may recrystallize quite differently. Without knowledge of the **starting texture, final**
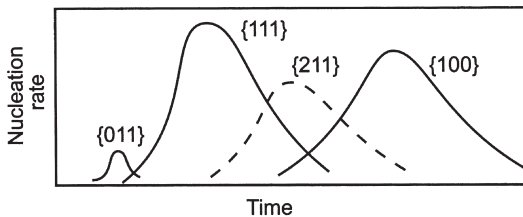

Fig. 7.8.   Schematic representation of the proposed orientation dependence of the nucleation rate in deformed iron, (after Hutchinson 1974).

texture and the orientation path linking them, it may not be possible to predict the recrystallization behaviour of a particular component of the deformation texture.
- The spatial distribution of orientations, which affects the grain boundary character distribution, will influence both the initiation and growth of recrystallized grains.

7.2.3 The original grain size

It is generally found that a fine-grained material will recrystallize more rapidly than a coarse-grained material, as seen in figure 7.9.

There are several ways in which the initial grain size may be expected to affect the rate of recrystallization.
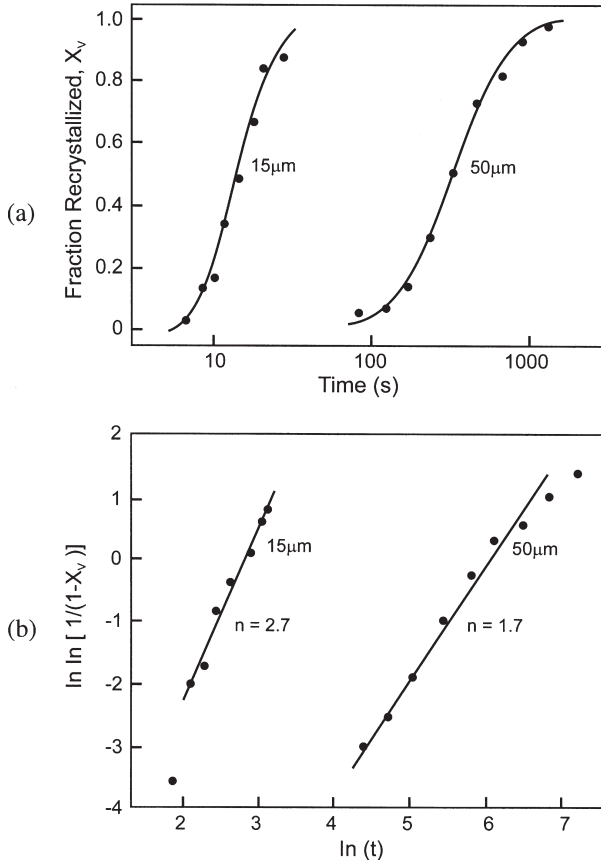

Fig. 7.9.   The recrystallization kinetics at 225°C of copper of different initial grain sizes cold rolled 93%: (a) fraction recrystallized, (b) JMAK plot, (Hutchinson et al. 1989a).

- The stored energy of a metal deformed to low strains ($\varepsilon < 0.5$) tends to increase with a decrease in grain size (§2.2.2).
- Inhomogeneities such as deformation and shear bands are more readily formed in coarse-grained material (e.g. Hatherly 1982) and thus the number of these features, which are also sites for nucleation, increases with increasing grain size (§2.7.4 and §2.8.4).
- Grain boundaries are favoured nucleation sites (§7.6.4), and therefore the number of available nucleation sites is greater for a fine-grained material.
- The deformation texture and hence the recrystallization texture may be influenced by the initial grain size, and as discussed above, the recrystallization kinetics will then be affected by the grain orientations.

Evidence for all of these effects may be found in the literature, although it should be noted that in the investigation of Hutchinson et al. (1989a) shown in figure 7.9, where the growth rate of the grains in the fine-grained material was some 20 times faster than that of the coarse-grained material at the same temperature, the difference in kinetics was ascribed primarily to orientation effects.

7.2.4 Solutes

The usual effect of solutes is to hinder recrystallization (Dimitrov et al. 1978). Table 7.2 shows the effect of zone refining on the recrystallization temperatures of various metals after large rolling reductions. Although the amount and type of impurities in the commercial materials is not specified, and in some cases they may contain second-phase particles, the marked effect of purifying the metals is clearly seen.

The quantitative effect of a solute on the recrystallization behaviour is dependent on the specific solvent/solute pair. A good example of a very potent solute which has an important influence on commercial alloys is iron in aluminium. Figure 7.10 shows how very small concentrations of iron in solid solution in high purity aluminium may increase the recrystallization temperature by $\sim100°C$.

An extensive survey of the effect of transition element solutes on the recrystallization of iron has been carried out by Abrahamson and colleagues (e.g. Abrahamson and

Table 7.2
The effect of purity on the temperature of recrystallization (Dimitrov et al. 1978).

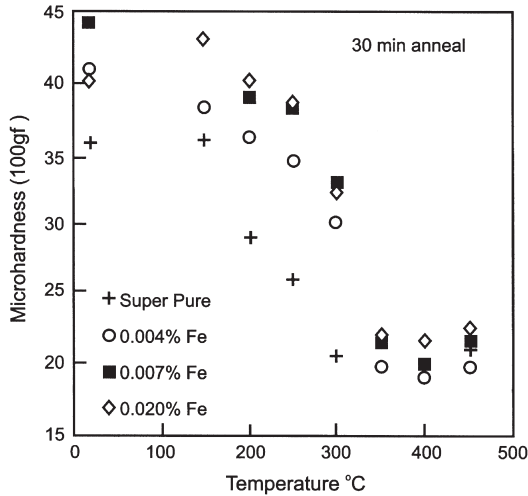| Metal	Recrystallization temperature (°C)	
	Commercial purity	Zone refined
Aluminium	200	−50
Copper	180	80
Iron	480	300
Nickel	600	300
Zirconium	450	170

Fig. 7.10.   The effect of trace amounts of iron in solid solution on the annealing response of aluminium deformed 80% by cold rolling, (Marshall and Ricks 1992).

Blakeny 1960). Although this work has indicated a correlation with the electron configuration of the solute, the effect remains unexplained.

Impurities may affect both the nucleation and growth of recrystallizing grains. It is difficult to measure or even define a **nucleation rate** for recrystallization, and the effect of impurities has not been quantified. Solutes may in some cases have a strong influence on the recovery processes which are an integral part of nucleation and which may affect the driving force for recrystallization. However, the majority of experimental work suggests that the main influence of solutes is on the grain boundary mobility (§5.3.3) and hence on the growth rate of recrystallizing grains (equation 7.1).

7.2.5 The deformation temperature and strain rate

At temperatures where thermally activated restoration processes such as dislocation climb occur during deformation, the microstructure will be dependent on the **deformation temperature** and **strain rate** in addition to the strain. After deformation at high temperatures and low strain rates, the stored energy will be reduced and recrystallization will occur less readily than after deformation to a similar strain at low temperature. These effects are considered in §13.6.

7.2.6 The annealing conditions

7.2.6.1 The annealing temperature
As may be seen from figure 7.11a, the annealing temperature has a profound effect on the recrystallization kinetics. If we consider the transformation as a whole and take the

time for 50% recrystallization ($t_{0.5}$) to be a measure of the rate of recrystallization, we might expect a relationship of the type:

$$\text{Rate} = \frac{1}{t_{0.5}} = C \exp\left(-\frac{Q}{kT}\right) \tag{7.5}$$

In figure 7.11b, we see that a plot of $\ln(t_{0.5})$ vs. $1/T$ gives a good straight line in accordance with equation 7.5, with a slope corresponding to an activation energy of 290 kJ/mol. Although such an analysis may be of practical use, an activation energy obtained from it is not easy to interpret, as it refers to the transformation as a whole,
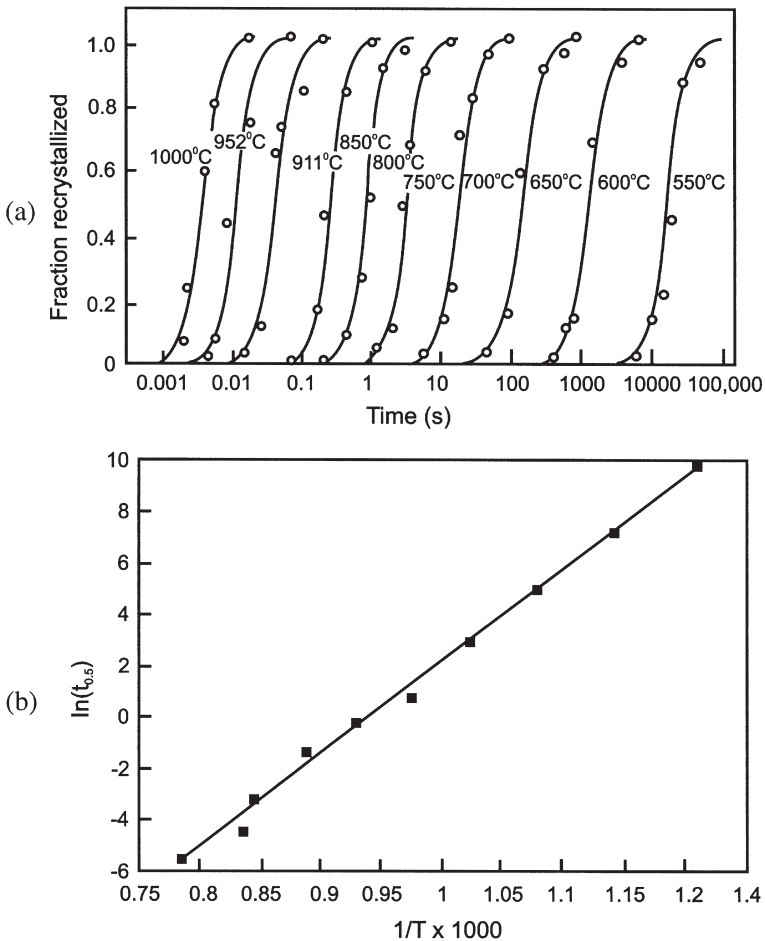

Fig. 7.11. (a) The effect of annealing temperature on the annealing of Fe-3.5%Si deformed 60%, (b) Arrhenius plot of the time for 50% recrystallization as a function of temperature, (data from Speich and Fisher 1966).

and is unlikely to be constant. For example such activation energies have been found to depend on strain (Gordon 1955) and to vary significantly with small changes in material purity. Vandermeer and Gordon (1963) found that an addition of only 0.0068 at% of copper to pure aluminium raised the activation energy for recrystallization from 60 to 120 kJ/mol.

An activation energy is only interpretable if it can be related to thermally activated processes at the atomic level. Consider the separate nucleation and growth processes which constitute recrystallization.

$$\dot{N} = C_1 \ \exp\left(-\frac{Q_N}{kT}\right) \qquad\qquad (7.6)$$

$$\dot{G} = C_2 \exp\left(-\frac{Q_G}{kT}\right) \qquad\qquad (7.7)$$

Although equation 7.7 has some validity because grain boundary migration rates are known to follow this type of relationship (§5.3.1), equation 7.6 is of little use because we have already noted that a constant nucleation rate is rarely found in practice. For example it was seen in §6.5 that the rate controlling process in recrystallization nucleation may be subgrain growth, in which case the activation energy for that process is the most relevant to nucleation.

7.2.6.2 The heating rate
The rate of heating of the specimen to the annealing temperature can also affect the rate of recrystallization. In order for this to occur, it is necessary for some other process to interact with recrystallization, and for this to have a different temperature dependence.

Consider the following two cases:

- **The heating rate affects the relative rates of recovery and recrystallization.**
If slow heating increases the amount of recovery occurring before recrystallization, the driving pressure will be reduced and recrystallization retarded. Although this effect is frequently cited in the literature, there is no experimental evidence to support it for single-phase alloys. Recovery would be enhanced at low heating rates only if it had a lower activation energy than recrystallization. In most alloys, the rates of both processes are controlled by lattice diffusion and have similar temperature dependencies; therefore heating rate is not predicted to affect one more than the other. In a very pure metal where HAGB migration is controlled by boundary diffusion (§5.3) and recovery by lattice diffusion, it would be expected that a low heating rate would in fact promote recrystallization, although this has not been reported.

- **Phase transformations can occur.**
Precipitation reactions have a different temperature dependence to recrystallization. If a supersaturated solid solution is deformed and annealed at a low heating rate, precipitation may occur before recrystallization and hinder it, whereas on rapid heating, recrystallization may be completed before any precipitation occurs. This effect, which is discussed in more detail in §9.8, may influence the rate of recrystallization in industrial

alloys, where it is often found that a rapid heating rate accelerates recrystallization and results in a smaller grain size, e.g. Al-Li alloys (Bowen 1990) and Al–Zn–Mg alloys (Wert et al. 1981).

Conversely, it is found that in steels, rapid heating may slow down recrystallization (Ushioda et al. 1989). In this case the heating rate determines the amount of carbon in solid solution, and this in turn affects the recrystallization (§15.3).

7.3 THE FORMAL KINETICS OF PRIMARY RECRYSTALLIZATION

7.3.1 The Johnson–Mehl–Avrami–Kolmogorov (JMAK) model

The type of curve shown in figure 7.3 is typical of many transformation reactions, and may be described phenomenologically in terms of the constituent nucleation and growth processes. The early work in this area is due to Kolmogorov (1937), Johnson and Mehl (1939) and Avrami (1939) and is commonly known as the JMAK model. A more general discussion of the theory of the kinetics of transformations may be found in the phase transformation literature, e.g. Christian (2002).

7.3.1.1 Theory
It is assumed that nuclei are formed at a rate $\dot{N}$ and that grains grow into the deformed material at a linear rate $\dot{G}$. If the grains are spherical, their volume varies as the cube of their diameter, and the fraction of recrystallized material (X_V) rises rapidly with time. However, the new grains will eventually impinge on each other and the rate of recrystallization will then decrease, tending to zero as X_V approaches 1.

The number of nuclei **(dN)** actually appearing in a time interval **(dt)** is less than $\dot{N}dt$ because nuclei cannot form in those parts of the specimen which have already recrystallized. The number of nuclei which would have appeared in the recrystallized volume is $\dot{N}X_V\,dt$ and therefore the total number of nuclei **(dN′)** which would have formed, including the 'phantom' nuclei is given by:

$$dN' = \dot{N}dt = dN + \dot{N}X_V\,dt \tag{7.8}$$

If the volume of a recrystallizing grain is **V** at time **t,** then the fraction of material which would have recrystallized if the phantom nuclei were real **(X_{VEX})** is known as the **extended volume** and is given by:

$$X_{VEX} = \int_0^t V dN' \tag{7.9}$$

If the incubation time is much less than **t,** then

$$V = f\dot{G}^3 t^3 \tag{7.10}$$

where $\mathbf{f}$ is a shape factor ($4\pi/3$ for spheres). Thus

$$X_{VEX} = fG^3 \int_0^t t^3 \dot{N}\, dt \qquad (7.11)$$

If $\dot{N}$ is constant then

$$X_{VEX} = \frac{f\dot{N}\dot{G}^3 t^4}{4} \qquad (7.12)$$

During a time interval $\mathbf{dt,}$ the extended volume increases by an amount $\mathbf{dX_{VEX}.}$ As the fraction of unrecrystallized material is $1 - X_V$, it follows that $\mathbf{dX_{VEX} = (1 - X_V)\,dX_{VEX},}$ or

$$dX_{VEX} = \frac{dX_V}{1 - X_V} \qquad (7.13)$$

$$X = \int_0^{X_V} dX_{VEX} = \int_0^{X_V} \frac{dX_V}{1 - X_V} = \ln\frac{1}{1 - X_V} \qquad (7.14)$$

$$X_V = 1 - \exp(-X_{VEX}) \qquad (7.15)$$

Combining equations 7.12 and 7.15

$$X_V = 1 - \exp\left(\frac{-f\dot{N}\dot{G}^3 t^4}{4}\right) \qquad (7.16)$$

This may be written more generally in the form

$$X_V = 1 - \exp(-Bt^n) \qquad (7.17)$$

where $B = f\dot{N}\dot{G}^3/4$, which is often called the **Avrami, Johnson–Mehl or JMAK equation.**

In the case considered above, in which the growing grains were assumed to grow in three dimensions, the exponent $\mathbf{n}$ in equation 7.17, which we will refer to as the **JMAK or Avrami exponent** is seen from equation 7.16 to be **4.** The above treatment assumed that the rates of nucleation and growth remained constant during recrystallization. Avrami (1939) also considered the case in which the nucleation rate was not constant, but a decreasing function of time, $\dot{N}$ having a simple power law dependence on time. In this situation $\mathbf{n}$ lies between 3 and 4, depending on the exact form of the function.

Two limiting cases are of importance, that already discussed in which $\dot{N}$ is constant and $\mathbf{n = 4,}$ and that where the nucleation rate decreases so rapidly that all nucleation events effectively occur at the start of recrystallization. This is termed **site saturated nucleation.**

Table 7.3
Ideal JMAK exponents.

Growth dimensionality	Site saturation	Constant nucleation rate
3-D	3	4
2-D	2	3
1-D	1	2

In this case, X_{VEX} in equation 7.12 is given by $fN(\dot{G}t)^3$ where N is the number of nuclei. This may be seen to give a JMAK exponent of **3** in equation 7.17.

The above analyses assume that until impingement, the grains grow isotropically in three-dimensions. If the grains are constrained either by the sample geometry or by some internal microstructural constraint to grow only in one or two-dimensions, then the JMAK exponent is lower as shown in table 7.3.

Cahn (1956) has extended the theory to include nucleation at random sites on grain boundaries and found that **n** fell from 4 at the start of the transformation to 1 at the end. However, no general analytical treatment of non-randomly distributed nucleation sites is available.

It should be noted that the essential feature of the JMAK approach is that the nucleation sites are assumed to be randomly distributed.

7.3.1.2 Comparison with experiment
Experimental measurements of recrystallization kinetics are usually compared with the JMAK model by plotting **ln[ln{1/(1 − X_V)}]** against **ln t.** According to equation 7.17, this should yield a straight line of slope equal to the exponent **n.** This method of data representation is termed a **JMAK plot.** It should incidentally be noted that equation 7.14 shows that this is equivalent to a plot of **ln X_VEX** against **ln t.**

The growth rate is not easily determined from measurements of X_V. However, if the interfacial area between recrystallized and unrecrystallized material per unit volume (S_V) is measured as a function of time, then Cahn and Hagel (1960) showed that the global growth rate $\dot{G}$ is given by

$$\dot{G} = \frac{1}{S_V}\frac{dX_V}{dt} \qquad (7.18)$$

There are a number of early experimental investigations of recrystallization in which JMAK kinetics were found with n ∼ 4. These include the work of Anderson and Mehl (1945) on aluminium, Reiter (1952) on low carbon steel and Gordon (1955) on copper. All these investigations were for fine-grained material deformed small amounts in tension. As pointed out by Doherty et al. (1986), in such conditions an increase in grain size on recrystallization is to be expected, with less than one successful nucleus arising
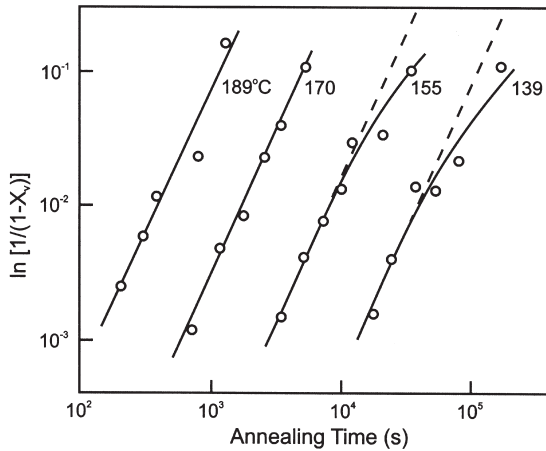
Fig. 7.12.   JMAK plot of the recrystallization kinetics of aluminium containing 0.0068 at.% Cu, deformed 40% by rolling, (Vandermeer and Gordon 1962).

from each old grain. Therefore the overall spatial distribution of these nuclei is likely to approach random (fig. 7.14a), thus fulfilling the conditions for JMAK kinetics. Figure 7.9b shows that the recrystallization behaviour of fine-grained copper is consistent with JMAK kinetics, whilst the logarithmic plot for the coarse-grained material demonstrates a strong negative deviation at long times.

It is in fact very unusual to find experimental data which, on detailed analysis, show good agreement with JMAK kinetics. Either the JMAK plot is non-linear, or the slope of the JMAK plot is less than 3, or both. A very clear example is the work of Vandermeer and Gordon (1962) on 40% cold rolled aluminium containing small amounts of copper, shown in figure 7.12. The JMAK slopes were found to be 1.7, and the data at the two lower annealing temperatures are seen to fall below the straight line at long annealing times. There are numerous investigation of aluminium and of other materials in which values of **n** of the order of 1 have been found. These include copper (Hansen et al. 1981) and iron (Michalak and Hibbard 1961, Rosen et al. 1964).

It is therefore concluded that the JMAK analysis discussed above is too simple to quantitatively model a process as complex as recrystallization. In particular, the change in microstructure during recrystallization needs to be described by more parameters than the fraction of material transformed (X_V or X_{VEX}).

7.3.2 Microstructural path methodology

A significant attempt to improve the JMAK approach was made by Vandermeer and Rath (1989a) using what they termed **Microstructural path methodology (MPM).** In this approach, more realistic and more complex geometric models are employed by using additional microstructural parameters in the analysis and, if required, relaxing the uniform grain impingement constraint.

As for the JMAK model, it is convenient to use the concept of **extended volume** (X_{VEX}) whose relation to the recrystallized fraction (X_V) is given by equation 7.15. In addition, the microstructure is characterised by the **interfacial area** per unit volume between recrystallized and unrecrystallized material (S_V) and this is related to the extended interfacial area (S_{VEX}) by the relationship (Gokhale and DeHoff 1985).

$$S_{VEX} = \frac{S_V}{1 - X_V} \tag{7.19}$$

As before, this relationship is valid only for randomly distributed recrystallized grains.

The growth of individual recrystallizing grains may be written in integral form

$$X_{VEX} = \int_0^t V_{(t-\tau)} \dot{N}_{(\tau)} \, dt \tag{7.20}$$

$$S_{VEX} = \int_0^t S_{(t-\tau)} \dot{N}_{(\tau)} \, dt \tag{7.21}$$

where $V_{(t-\tau)}$ and $S_{(t-\tau)}$ are the volume and interfacial area respectively at time **t**, of a grain which was nucleated at time τ.

If it is assumed that the grains are spheroids which do not change shape, then the volume and interfacial area of a grain are

$$V_{(t-\tau)} = K_V \cdot a_{(t-\tau)}^3 \tag{7.22}$$

$$S_{(t-\tau)} = K_S \cdot a_{(t-\tau)}^2 \tag{7.23}$$

where **a** is the major semi-axis of the spheroid and K_V and K_S are shape factors. The radius function $a_{(t-\tau)}$ is related to the interface migration rate G(t) by

$$a_{(t-\tau)} = \int_\tau^t G(t) \, dt \tag{7.24}$$

Whereas X_{VEX} and S_{VEX} are global microstructural parameters which may be measured metallographically, $a_{(t-\tau)}$ is a local property, and may be estimated by measuring the diameter of the largest unimpinged grain intercept (D_L) on a plane polished surface. If it can be assumed that this is the diameter of the earliest nucleated grain, then $a_{(t-\tau)} = D_L/2$.

Vandermeer and Rath (1989a), using the method of Gokhale and DeHoff (1985) have shown that the nucleation and growth characteristics of the recrystallizing material are contained in the time dependence of equations 7.20 and 7.21, and have demonstrated how these equations may be evaluated to extract the **nucleation rate, growth rate,** and **size** of the recrystallizing grains. The method involves inverting the equations, based on the mathematics of Laplace transforms.

For isothermal annealing, it is assumed that the time dependence of X_{VEX}, S_{VEX} and D_L may be represented by power law functions of the form

$$X_{VEX} = Bt^n \qquad (7.25)$$
$$S_{VEX} = Kt^m \qquad (7.26)$$
$$D_L = St^s \qquad (7.27)$$

It is also postulated that the derived functions can be represented by power law functions, thus

$$\dot{N}_{(\tau)} = N_l \tau^{\delta-1} \qquad (7.28)$$
$$a_{(t-\tau)} = G_a(t - \tau)^r \qquad (7.29)$$

where N_l, G_a δ and r are constants.

If the shapes of the grains remain spheroidal during growth then $a_{(t)} = D_L/2$ and hence $r = s$ and $G_a = S/2$.

Vandermeer and Rath show that for spheroidal grains which retain their shape during growth

$$\delta = 3m - 2n \qquad (7.30)$$
$$r = s = n - m \qquad (7.31)$$

Reference to equations 7.25–7.29 shows that:

$\delta = 1$ corresponds to a constant nucleation rate
$\delta = 0$ to site saturated nucleation
$r = s = 1$ corresponds to a constant growth rate.

Therefore, by measuring X_V, S_V and D_L experimentally as a function of annealing time, **n, m** and **s** may be determined, δ and **r** calculated and the form of the nucleation kinetics identified.

If the simple JMAK model discussed above applies, then, for constant nucleation and growth rates we would obtain $n = 4$, $m = 3$, $s = 1$ and hence $\delta = 1$ and $r = 1$.

Figure 7.13, from the work of Vandermeer and Rath shows data for the recrystallization of a deformed iron crystal plotted to give n, m and s from the slopes of the lines in figures 7.13a, b, c respectively. The data have been normalised using an Arrhenius relationship so as to include results obtained at several temperatures. The values obtained are $n = 1.90$, $m = 1.28$, $s = 0.60$, which give $\delta = 0.04$ and $r = 0.62$. As δ is almost zero, it is concluded that nucleation is effectively site saturated, and as $r \sim s$ it is concluded that the grains grow as spheroids. The low value of **r** indicates a growth rate decreasing with time.

If $s \neq r$ then the grain shape is changing during recrystallization, and further information about the shapes of the grains may be extracted (Vandermeer and Rath 1990).
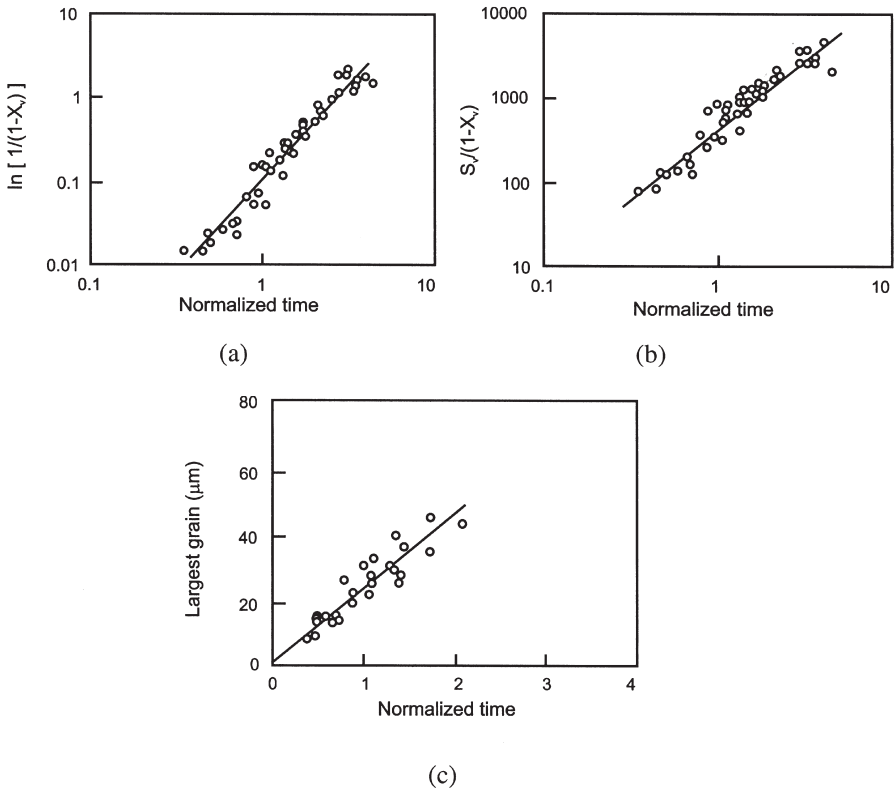
Fig. 7.13.   Annealing kinetics of an iron crystal deformed 70% and annealed at various temperatures. By normalising the time axis by means of an Arrhenius relationship, data from a range of annealing temperatures are found to fall on a common curve. (a) Variation of X_V, (b) variation of S_V, (c) variation of largest recrystallized grain diameter, (Vandermeer and Rath 1989a).

The model has also been extended to include the effects of recovery during the recrystallization anneal (Vandermeer and Rath 1989b).

Microstructural path methodology allows more detailed information about nucleation and growth rates to be extracted from experimental measurements than does the original JMAK analysis, and is a very useful tool in determining whether or not nucleation is site-saturated (e.g. Vandermeer and Juul Jensen 2001). However, it should be noted that whilst the MPM approach is more flexible than the JMAK model, it is still based on the assumption that the spatial distribution of nuclei is random and that growth rates are global rather than local parameters.

From the above discussion of the JMAK and MPM models it is clear that the two factors most likely to cause problems in realistic modelling of recrystallization kinetics

are **inhomogeneous recrystallization** and **concurrent recovery,** and these are considered in the next section.

7.4 RECRYSTALLIZATION KINETICS IN REAL MATERIALS

7.4.1 Non-random spatial distribution of nuclei

It is widely recognised that the nucleation sites in recrystallization are non-randomly distributed. However, the analytical treatments of kinetics discussed above are unable to satisfactorily take this into account.

Evidence for non-random site distribution is found for all materials, particularly those with a large initial grain size, and examples include **iron** (Rosen et al. 1964), **copper** (Hutchinson et al. 1989a), **brass** (Carmichael et al. 1982) and **aluminium** (Hjelen et al. 1991, Somerday and Humphreys 2003b).

On the scale of a single grain, nucleation of recrystallization is inhomogeneous as is discussed in more detail in §7.6. Nucleation occurs at preferred sites such as prior grain boundaries, at transition bands, and shear bands. At lower strains, fewer of these deformation heterogeneities are formed and fewer of those formed act as nucleation sites. Whether or not these small-scale inhomogeneities lead to an overall inhomogeneous distribution of nuclei will depend on the number of nuclei relative to the number of potential sites, as shown schematically in figure 7.14. If nucleation only occurs at grain boundaries, then a given number of nuclei in a fine-grained material (fig. 7.14a) will lead to more homogeneous recrystallization than the same number in a coarse-grained material (fig. 7.14b). The limiting case is that of single crystals in which recrystallization nucleation is rarely randomly distributed (e.g. Driver 1995, Mohamed and Bacroix 2000, Driver et al. 2000, Godfrey et al. 2001).

On a larger scale, it is also found, that not all grains in a material recrystallize at a similar rate, and it is this larger-scale heterogeneity that is frequently the main cause of
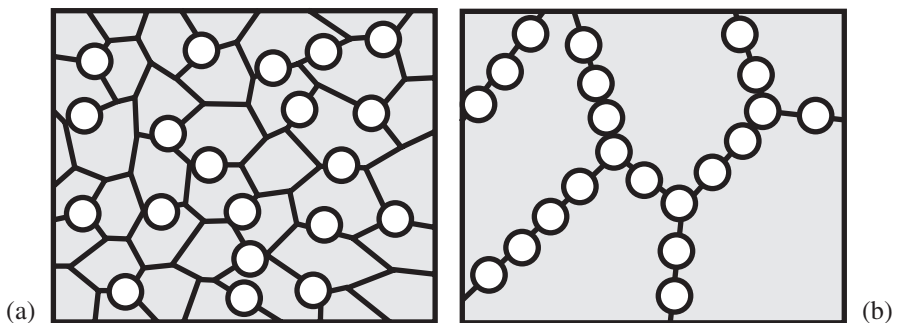

Fig. 7.14.   Schematic representation of the effect of the initial grain size on the heterogeneity of nucleation. (a) Small initial grain size, (b) large initial grain size.
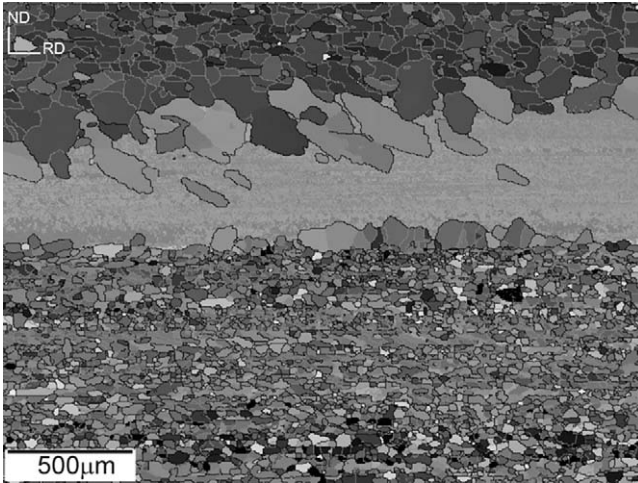
Fig. 7.15.   EBSD map of a cold rolled single-phase, coarse-grained Al-0.05 wt%Mn
alloy which has been partially recrystallized. The area originally contained three
deformed grains. The upper and lower grains have recrystallized to different grain sizes,
whilst no recrystallization has occurred in the central (Goss-oriented) grain. The colours
represent the orientations within the sample, (Somerday and Humphreys 2003b).
(See colour plate section.)

inhomogeneous recrystallization. This effect arises from the orientation differences
between grains. As discussed in chapter 2, the slip systems and strain path which operate
during deformation are dependent on crystallographic orientation. Thus the distribu-
tion and density of dislocations and of larger scale microstructural inhomogeneities is
orientation dependent. Therefore the availability and viability of nucleation sites and
also the growth rate of the recrystallizing grains depends strongly on orientation.

Fcc crystals of the {110} <001> Goss orientation deformed in plane strain compression
are an extreme example. In these materials no deformation heterogeneities form and no
recrystallization is nucleated (Ferry and Humphreys 1996a). Goss-oriented grains in a
deformed fcc polycrystal are also slow to recrystallize, and figure 7.15 shows an EBSD
map of a deformed large-grained single-phase aluminium alloy which has partially
recrystallized on annealing. The area of the sample originally comprised three grains,
whose boundaries were aligned in the rolling direction (RD). The lower grain has
recrystallized to a grain size of ~15 µm and the upper grain has recrystallized to a grain
size of ~30 µm. No recrystallization has originated in the central Goss-oriented grain,
but some large (~100 µm) grains from the upper and lower grains are growing into the
Goss grain.

An extreme example of inhomogeneous recrystallization is found in low zinc α-brass
(Carmichael et al. 1982) in which, depending on their initial orientation, grains may
deform either by reasonably uniform slip or by deformation twinning and shear
banding. On annealing, the latter grains recrystallize first and are often completely
recrystallized before the former have started to recrystallize as shown in figure 7.16b.
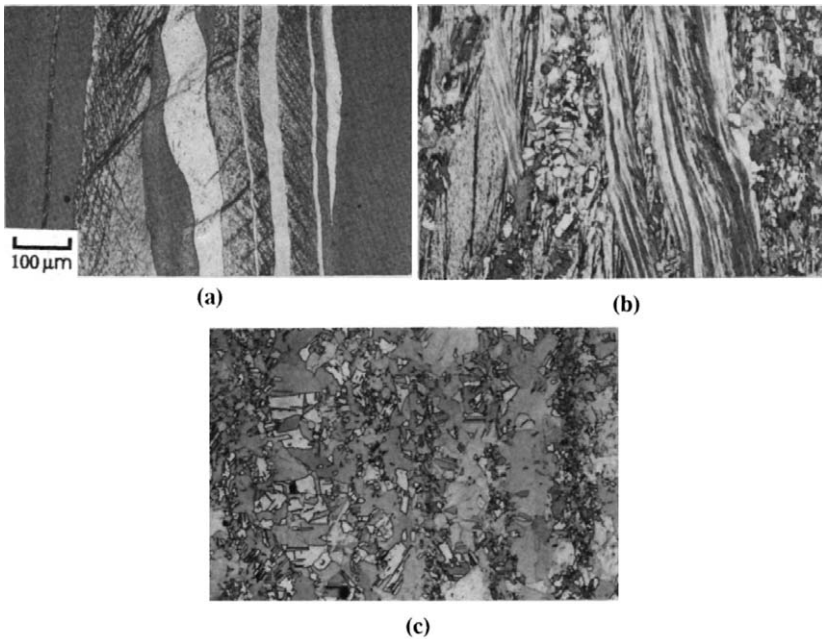
Fig. 7.16.   Inhomogeneous recrystallization in 95:5 brass cold rolled 75% and annealed, (TD section with rolling direction vertical); (a) as deformed, (b) 6 min at 250°C, (c) 24 hr at 250°C, (Carmichael et al. 1982).

In alloys containing large second-phase particles which stimulate the nucleation of recrystallization (§9.3.4), clustering of the particles may, for similar reasons, lead to macroscopically inhomogeneous recrystallization.

7.4.2 The variation of growth rate during recrystallization

7.4.2.1 Experimental observations
There is considerable evidence that the growth rate $(\dot{G})$ is not a constant, and therefore a realistic treatment of recrystallization kinetics must allow for the variation of $\dot{G}$ in both space and time. Although there may be some variation of the boundary mobility **(M)** during recrystallization, for example through an orientation dependence of mobility (§5.3.2), the main reason for such changes in growth rate is thought to be variations in the **driving pressure.** The driving pressure may vary through the material due to microstructural inhomogeneity and may also decrease with time due to recovery occurring concurrently with recrystallization. It is now thought that in many cases **both** these effects occur, making the interpretation or prediction of growth rates very difficult.

There have been several detailed measurements of grain boundary velocities during recrystallization, including those on **aluminium** (Vandermeer and Gordon 1959, Furu

and Nes 1992), **iron** (Leslie et al. 1963, English and Backofen 1964, Speich and Fisher 1966, Vandermeer and Rath 1989a) and **titanium** (Rath et al. 1979). The growth rates were usually determined either by measurement of the size of the largest growing grain, or by the Cahn–Hagel analysis (equation 7.18). In all these investigations the growth rates were found to decrease significantly with annealing time.

Various equations have been used to express the variation of $\dot{\mathbf{G}}$ with time such as

$$\dot{\mathbf{G}} = \frac{A}{1 + Bt^r} \qquad (7.32)$$

which, at long times reduces to

$$\dot{\mathbf{G}} = Ct^{-r} \qquad (7.33)$$

In several cases **r** has been found to be close to 1, although in their investigation of the recrystallization kinetics of iron, Vandermeer and Rath (1989a) found r $= 0.38$.

The basic JMAK model of §7.3.1 assumes a constant growth rate, and the following analysis illustrates the effect of recovery on the growth rate and on the kinetics of recrystallization. More detailed treatments are discussed by Furu et al. (1990).

If we allow $\dot{\mathbf{G}}$ to vary, then for site-saturated nucleation with **N** nuclei, equation 7.16 becomes

$$X_v = 1 - \exp\left[-f\,N\left(\int_0^t \dot{\mathbf{G}}\mathbf{dt}\right)^3\right] \qquad (7.34)$$

If the variation of growth rate with time is as given by equation 7.33, then combining equations 7.33 and 7.34 we find

$$X_v = 1 - \exp\left[-f\,N\left(C\frac{t^{(1-r)}}{(1-r)}\right)^3\right] \qquad (7.35)$$

The JMAK plots for the recrystallization kinetics given by equation 7.35 are shown in figure 7.17 for various values of **r**.

Note that as the growth rate is increasingly slowed (increasing **r**), the JMAK plot remains a straight line. However the slope decreases and, from equation 7.35 is equal to $3(1-r)$.

7.4.2.2 The role of recovery

Until recently, a decreasing growth rate during recrystallization or a non-linear JMAK plot was thought to be due entirely to the effects of recovery on the driving force for recrystallization. The classic early work in this field is that of Vandermeer and Gordon
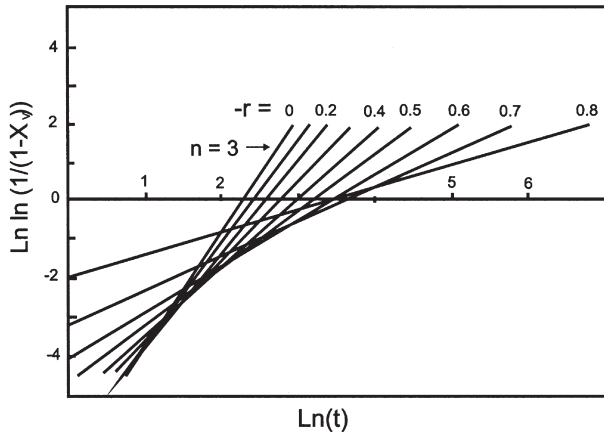
Fig. 7.17.   The predicted effect of the recovery parameter **r** in equation 7.35 on the JMAK plot for recrystallization under conditions of site saturated nucleation.

(1962) who carried out an extensive metallographic and calorimetric study of the recrystallization of aluminium alloys containing small amounts of copper. In this work the low JMAK slopes and the deviation of these plots from linearity at long times (fig. 7.12) were attributed to recovery. However, it is now thought that in many cases, factors other than recovery may be more important.

Consider the measurements of the softening during annealing of cold worked copper and aluminium shown in figure 7.18. For the case of copper (fig. 7.18a) there is no softening prior to that due to recrystallization, but for aluminium (fig. 7.18b), there is extensive prior softening, and these observations are consistent with our knowledge of recovery in these materials. Although we may expect some recovery during the recrystallization of aluminium which will lower the driving force, it is unlikely that there will be significant recovery in copper, or other metals of medium to low stacking fault energy. In such materials, recovery is not a likely explanation for the low JMAK exponents, nor the non-linearity of the JMAK plots at longer times, such as shown in figure 7.9b.

We must now question the role of recovery in affecting recrystallization even in those materials for which recovery is known to occur readily.

Would uniform recovery explain the observed JMAK plots?
As discussed in chapter 6, recovery lowers the driving pressure (P) for recrystallization and is therefore expected to reduce $\dot{\mathbf{G}}$ according to equation 7.1. Although our knowledge of recovery kinetics is far from complete, the available evidence suggests that recovery processes are broadly consistent with the kinetics of growth rate reduction as given by equations 7.32 and 7.33. For example a JMAK slope of 2, which is commonly observed experimentally, implies a not unreasonable value of $r = 0.33$ in equation 7.33. However, recovery on the model discussed above or on the model of Furu et al. (1990), leads to linear JMAK plots and would therefore not explain the frequent observation of non-linearity such as shown in figure 7.12.
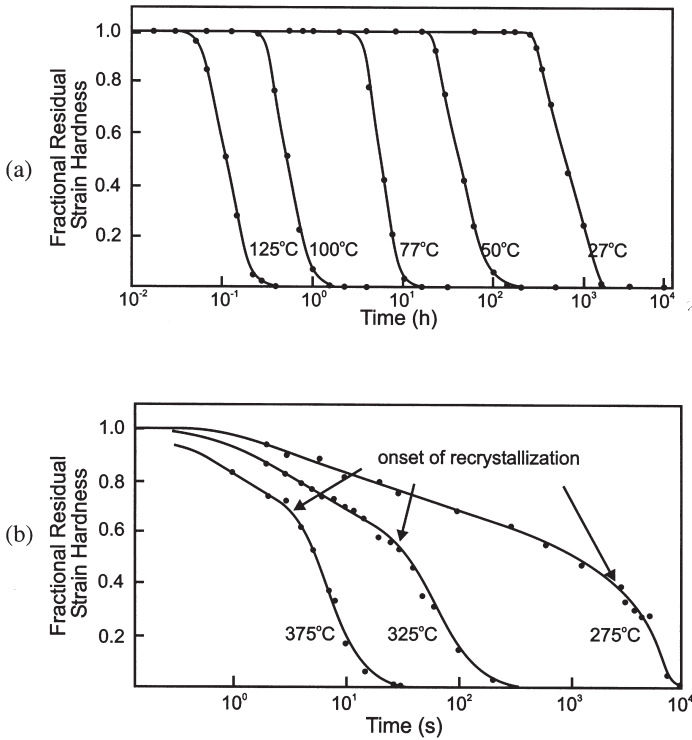
Fig. 7.18.   The variation of the fractional residual strain hardening during annealing for (a) cold worked copper (Cook, and Richards 1946) and (b) commercial purity aluminium, (Furu et al. 1990).

Is the temperature dependence of $\dot{G}$ consistent with recovery?

In their investigation of the recrystallization kinetics of iron, Vandermeer and Rath (1989a) found that data over a wide range of annealing temperatures could be fitted to equation 7.33 if the data were normalised to take account of the temperature dependence of the growth rate (fig. 7.13c). If this decrease in growth rate were due to recovery, then it would fit equation 7.33 over the whole temperature range only if the activation energies for recovery and high angle grain boundary migration were equal. As discussed in §7.2.6.2, this is probable, with both processes being controlled by lattice diffusion, although it would also be consistent with the microstructural inhomogeneity discussed in the following section.

Is the amount of recovery sufficient to explain the recrystallization kinetics?

Several investigations (e.g. Perryman (1955) on aluminium and Rosen et al. (1964) on iron), have indicated that prior recovery treatment has little effect on recrystallization. In figure 7.19, the JMAK plots for iron which had been recovered at various temperatures before recrystallization, show that prior recovery has had little effect on the recrystallization kinetics.
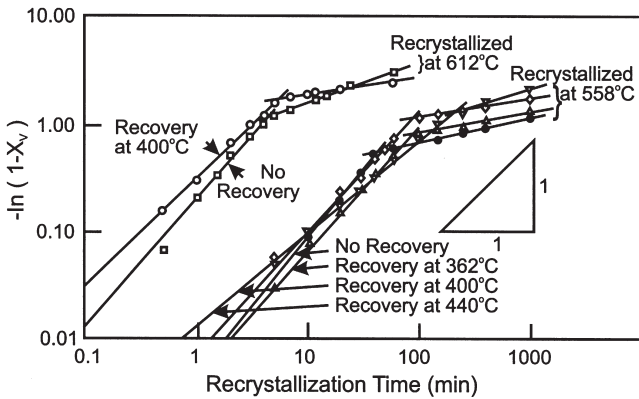
Fig. 7.19.   The effect of recovery on the recrystallization of iron, (Rosen et al. 1964).

More recent experimental measurements of both the extent of recovery and the growth rate of recrystallization in aluminium (Furu and Nes 1992) have shown that the amount of uniform recovery is relatively small (20% at $X_V = 0.1$) and is not in itself sufficient to account for the observed decrease of the growth rate.

It is therefore likely that factors other than recovery are contributing to the decrease in growth rate at long annealing times.

7.4.2.3 The role of microstructural inhomogeneity
The nature of the deformation microstructure (§2.4) gives rise not only to the inhomogeneous distribution of recrystallization nuclei discussed in §7.4.1, but also to the variations in stored energy which are responsible for inhomogeneous growth rates.

Hutchinson et al. (1989a) investigated inhomogeneous recrystallization in cold rolled OFHC copper. They measured the release of stored energy during the recrystallization, and found that it was not proportional to the fraction recrystallized, and that the regions of high stored energy recrystallized first (fig. 7.20a). The measured growth rate of the recrystallizing grains decreased with time, and they were able to show that this was due entirely to the inhomogeneity of the stored energy distribution. As shown in figure 7.20b, the mean growth rate was found to be proportional to the true driving force, which was calculated from the calorimetric measurements. The recrystallization kinetics from this work, shown in figure 7.9b, indicate that although the fine-grained material gave a linear JMAK plot with a slope of 2.7, the coarse-grained material, in which the recrystallization was more inhomogeneous had a significantly lower slope of 1.7 and the data fell well below the straight line plot during the later stages of recrystallization.

Earlier work on aluminium (Vandermeer and Gordon 1962), also showed that the amount of heat evolved per unit volume recrystallized, decreased as recrystallization proceeded. Although this was interpreted as being due to recovery, it is quite possible
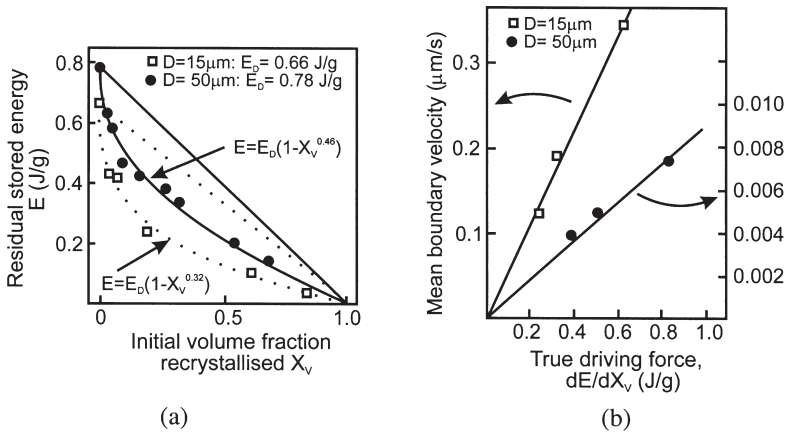
Fig. 7.20. The effect of the inhomogeneous distribution of stored energy on the recrystallization of the copper specimens whose kinetics are shown in figure 7.9. (a) Correlation of the residual stored energy and the volume fraction recrystallized shows that a large part of the stored energy is released during the early stages of recrystallization, (b) correlation of the growth rate and the rate of decrease of stored energy shows the boundary velocity to be approximately proportional to the driving force, (Ryde et al. 1990).

that these results could also be explained at least in part, by an inhomogeneous distribution of stored energy.

As deformation microstructures are very varied and not well understood, it is difficult to give a general treatment of recrystallization in inhomogeneous microstructures, although specific cases have been modelled analytically by Vandermeer and Rath (1989b) and Furu et al. (1990).

In figure 7.21 we schematically illustrate one possible case. In figure 7.21a, spherical regions of high stored energy (dark shaded) are present in the deformed microstructure. These might for example, correspond to the highly deformed regions associated with large second-phase particles (§2.9.4). If recrystallization nucleates predominantly in or close to these regions then growth will be initially rapid, but will decrease when these regions of high stored energy are consumed (fig. 7.21b). In this case the heterogeneity is **local** and if the stored energy within these regions can be calculated, the growth rate and hence the recrystallization kinetics may be modelled analytically (Furu et al. 1990) on the basis of equation 7.34. Vandermeer and Juul Jensen (2001) interpreted the two-stage growth kinetics observed during recrystallization of an aluminium alloy in which nucleation occurred at large second-phase particles (see §9.3) in terms of such a model.

However, if few nuclei are formed, for example after low strains (fig. 7.21c), then growing grains will experience a driving force which is an average of the high and low energy regions and which will not vary during the recrystallization.
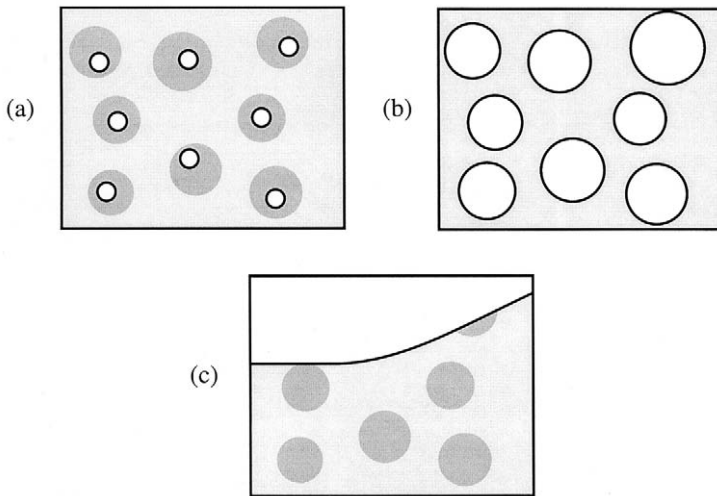
Fig. 7.21.   The effect of local variations of stored energy on recrystallization. (a) If nucleation (white areas) occurs in regions of high stored energy (dark areas) then the growth rate diminishes as recrystallization proceeds, (b) after the regions of high stored energy are consumed, (c) if recrystallization nucleation is on a coarser scale than the distribution of stored energy then the growing grains sample an average stored energy which remains approximately constant as recrystallization proceeds.
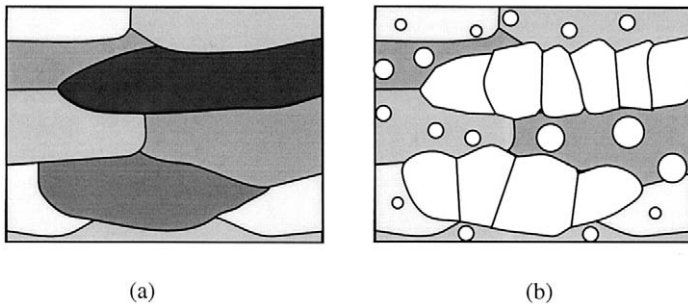

Fig. 7.22.   A variation of stored energy from grain to grain as shown in (a), where regions of higher stored energy are shaded darker, results in inhomogeneous grain growth during recrystallization as shown in (b).

In figure 7.22, we illustrate a situation in which the deformed grains have different microstructures and stored energies. In this case the heterogeneity is on a much **coarser scale** than the example of figure 7.21. Even if nucleation is relatively uniform, growth will occur most rapidly in the grains of highest stored energy, leading to the type of microstructures shown in figure 7.22b. In this case not only will the growth rate decrease during recrystallization as the higher stored energy regions are

consumed, but growth of the grains will be restricted by impingement with their neighbours within the original grains.

Although analytical modelling cannot easily deal with the kinetics of inhomogeneous recrystallization, computer simulations of the type discussed in chapter 16 may be used to address the problem (Rollett et al. 1989a, Furu et al. 1990). As may be seen from the simulations of figure 16.13, inhomogeneous distribution of nuclei leads not only to low values of the JMAK slope, in agreement with many experimental measurements, but also to a decrease of the JMAK slope as recrystallization proceeds.

Thus we conclude that the deviation of recrystallization kinetics from the ideal linear JMAK plots and the low values of the exponent which are found in many experimental investigations, are in most cases directly attributable to the inhomogeneity of the microstructure. This leads to non-random distribution of nucleation sites and stored energy and to a growth rate which decreases with time.

7.5 THE RECRYSTALLIZED MICROSTRUCTURE

7.5.1 The grain orientations

In general the recrystallized grains are not randomly oriented, but have a **preferred orientation** or **texture.** The origin of recrystallization textures is discussed in detail in chapter 12, and some examples of texture control in industrial practice are given in chapter 15.

7.5.2 The grain size

The magnitude of the final grain size can be rationalised in terms of the effects of the various parameters on the nucleation and growth processes. Any factor such as a high strain or a small initial grain size, which favours a large number of nuclei or a rapid nucleation rate, will lead to a small final grain size as illustrated for α-brass in figure 7.23, where it may be seen that the annealing temperature has little effect on the final grain size. However if a change of annealing temperature or heating rate alters the balance between nucleation and growth, which is most likely in two-phase alloys (§7.2.6), then the final grain size will be affected accordingly.

The grain size may not be constant throughout a specimen. Just as the different texture components within a specimen recrystallize at different rates (§7.4), so the final grain size and shape within each texture component may be different as seen in figures 7.15, 7.16 and 7.25.

The spectrum of grain sizes as measured on a plane section is usually found to be close to a log normal distribution as shown in figure 7.24, and a similar grain size distribution has been reported for partly recrystallized material (Marthinsen et al. 1989).
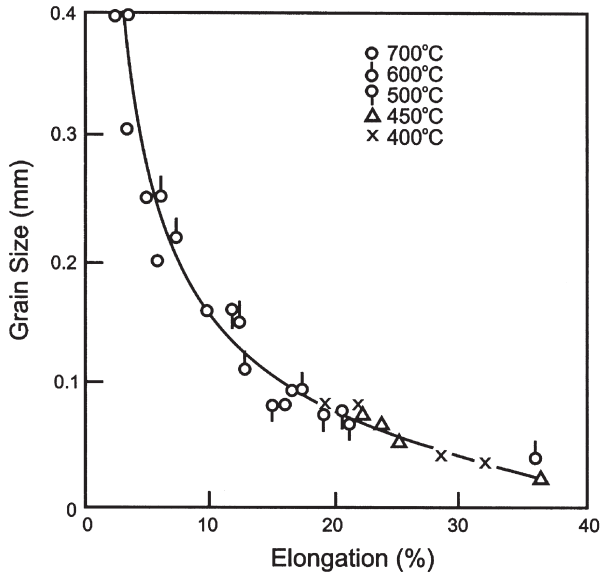
Fig. 7.23.   The effect of tensile strain on the final grain size in α-brass recrystallized at various temperatures, (Eastwood et al. 1935).
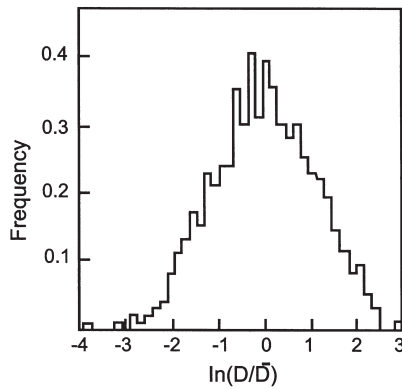

Fig. 7.24.   The experimentally measured grain size distribution following the recrystallization of an Al-0.3%Fe alloy, (Saetre et al. 1986a).

7.5.3 The grain shape

If grains are uniformly distributed and growth is isotropic then the recrystallized structure consists of equiaxed polyhedra (§4.5). Although in many cases the recrystallized grains are approximately equiaxed, there are some instances where anisotropic growth leads to plate-shaped grains as may be seen in figures 7.15 and 7.25.
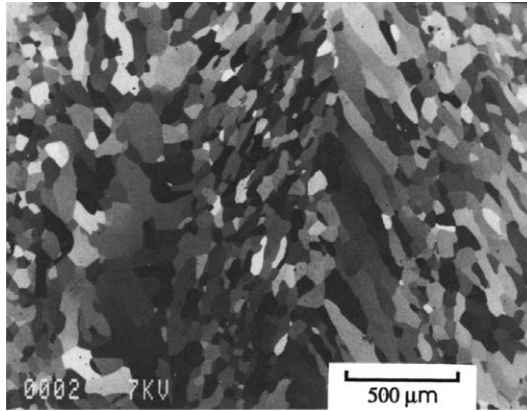
Fig. 7.25.   SEM channelling contrast image of recrystallized high purity aluminium,
showing the effect of anisotropic grain growth during recrystallization,
(Hjelen et al. 1991).

This type of growth anisotropy is often crystallographic, and a particularly important case is for grains of fcc metals oriented by $\sim 40°$ about a $<111>$ axis to the deformed matrix. In this situation, which is discussed in more detail in §5.3.2 and §12.3.2, the sides of a growing grain which form **tilt boundaries** to the deformed grain grow much faster than the other faces, resulting in plate-shaped grains such as that shown in figure 5.14. However, because such preferential growth is restricted to only tilt boundaries of very specific orientation relationships, it may not have a significant influence on the microstructure of recrystallized polycrystals.

In industrial, particle-containing alloys, anisotropic distribution of the particles, often along planes parallel to the rolling plane may reduce the growth rate perpendicular to the rolling plane as discussed in §4.6.2.3, resulting in pancake grains after recrystallization as shown in figure 4.28.

7.6 THE NUCLEATION OF RECRYSTALLIZATION

There has been a considerable research effort aimed at trying to understand the processes by which recrystallization originates. The importance of recrystallization nucleation is that it is a critical factor in determining both the size and orientation of the resulting grains. In order to control recrystallization effectively, it is necessary to understand the mechanisms of nucleation and the parameters which control it.

7.6.1 Classical nucleation

The possibility that the classical nucleation theory developed for phase transformations might be applicable to recrystallization was considered by Burke and Turnbull (1952).

In this situation, nucleation would be accomplished by random atomic fluctuations leading to the formation of a small crystallite with a high angle grain boundary. Such a nucleus would be stable if the difference in energy between the local deformed state and the recrystallized state were larger than the energy of the high energy interface produced in forming the nucleus. Although this theory appears to account for some aspects of recrystallization, such as the incubation period and preferential nucleation at regions of high local strain, it can be discounted because:

- **The driving force is low.** In comparison with phase transformations, the energy which drives the recrystallization process is very small (§2.2.1).
- **The interfacial energy is large.** The energy of a high angle grain boundary, which is an essential factor in the recrystallization process, is very large (§4.4.3).

Calculations based on nucleation theory (see e.g. Christian 2002) indicate that the radius of the critical nucleus (greater than 0.1 μm), is so large that the rate of nucleation will be negligible, and that this is therefore not a viable mechanism for the origin of recrystallization.

It is now accepted that the 'nuclei' from which recrystallization originates are therefore not nuclei in the strict thermodynamic sense, but small volumes which pre-exist in the deformed microstructure.

7.6.2 Strain induced grain boundary migration (SIBM)

This mechanism, an example of which is seen in figure 7.26 was first reported by Beck and Sperry (1950) and has been observed in a wide variety of metals. SIBM involves the bulging of part of a pre-existing grain boundary, leaving a region behind the migrating boundary with a lower dislocation content as shown schematically in figure 7.27. A characteristic feature of this mechanism is that the new grains have similar orientations
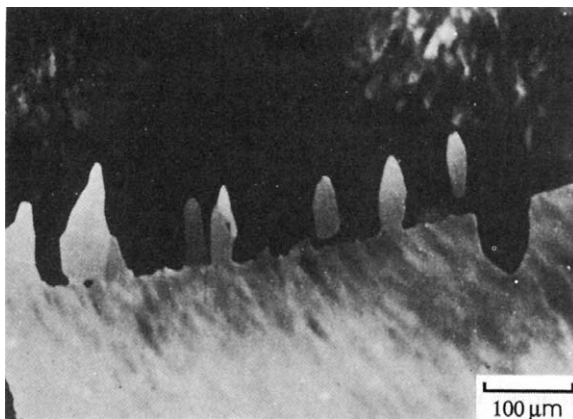

100 μm

Fig. 7.26.   An optical micrograph showing strain-induced grain boundary migration in aluminium, (Bellier and Doherty 1977).

(a)   (b)
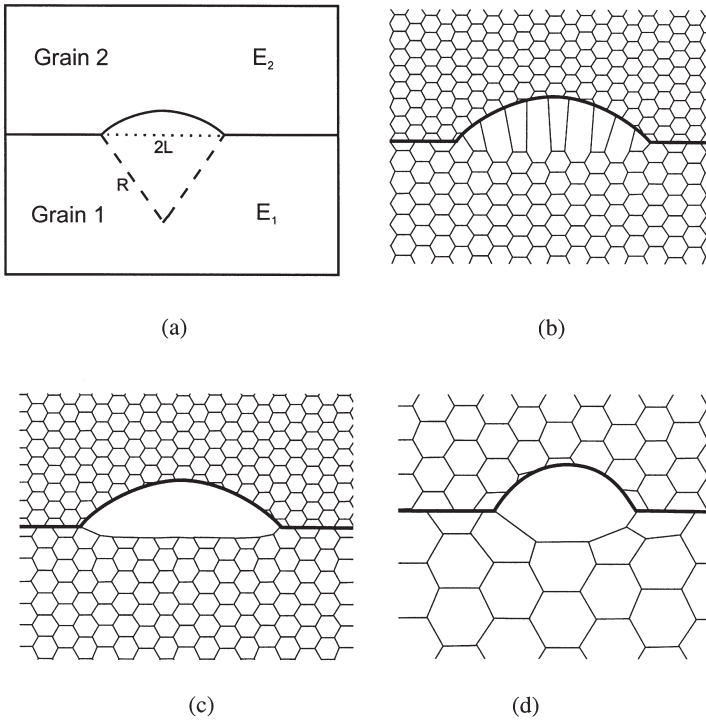

(c)   (d)

Fig. 7.27.   (a) SIBM of a boundary separating a grain of low stored energy (E$_1$) from one of higher energy (E$_2$), (b) dragging of the dislocation structure behind the migrating boundary, (c) the migrating boundary is free from the dislocation structure, (d) SIBM originating at a single large subgrain.

to the old grains from which they have grown. This mechanism is particularly important after low strains, and Beck and Sperry found that at reductions $>40\%$ in pure aluminium the mechanism was apparently replaced by one in which grains of orientations different from either of the matrix grains were formed (see §7.6.4). In the early work, the similarity or otherwise of the new and old grain orientations was inferred from the contrast produced by etching, which may not be reliable. However, Bellier and Doherty (1977) were able to determine the grain orientations and, in rolled aluminium, confirmed that SIBM was the dominant recrystallization mechanism for reductions of less than 20%. Because of the orientation relationship between the new and old grains, operation of this mechanism is expected to result in a recrystallization texture which is closely related to the deformation texture. More recent research has shown that SIBM is also very important during recrystallization after high temperature deformation of aluminium and steels, when the deformation microstructures are more homogeneous than after lower temperature deformation (e.g. Theyssier and Driver 1999, Hutchinson et al. 1999b). The strengthening of the $\{100\}<001>$ **cube texture** during the recrystallization of aluminium alloys after high temperature deformation, which is of great industrial significance and which is discussed in (§12.4.1), is known to

be due to SIBM at the boundaries of cube-oriented regions in the deformed microstructure (e.g. Vatne and Nes 1994, Vatne et al. 1996a, 1996d).

7.6.2.1 Multiple subgrain SIBM

The driving force for SIBM is usually presumed to arise from a difference in dislocation content on opposite sides of the grain boundary. This could result directly from the deformation process, because it is known that the dislocation storage rate may be dependent on grain orientation (§2.2.3.3) and may also be different in the boundary regions.

The kinetics of the process were first analysed by Bailey and Hirsch (1962). In figure 7.27a, if the deformed grains have stored energies of E_1 and E_2 and $E_1 < E_2$, then the driving force is provided by the energy difference $\Delta E = E_2 - E_1$. If the bulging boundary is a spherical cap of radius **R,** with a specific boundary energy γ_b, the interfacial energy of the bulging region of the boundary is given by

$$E_B = 4\pi R^2 \gamma_b \qquad (7.36)$$

and

$$\frac{dE_B}{dR} = 8\pi R \gamma_b \qquad (7.37)$$

In the early stages of bulging, the energy difference per unit volume across the boundary is ΔE and

$$\frac{dE}{dR} = 4\pi R^2 \Delta E \qquad (7.38)$$

For the bulge to grow $dE/dR > dE_B/dR$ and hence

$$R > \frac{2\gamma_b}{\Delta E} \qquad (7.39)$$

This reaches a critical value when the boundary bulge becomes hemispherical, when $R = R_{crit} = L$, and

$$R_{crit} > \frac{2\gamma_b}{\Delta E} \qquad (7.40)$$

On its concave side, the bulging boundary is joined to the lower grain by an array of dislocations or low angle boundaries, and it is not at all clear whether at the critical stage (equation 7.40), the boundary can still be considered as separating regions of high stored energy (E_1 and E_2) as shown in figure 7.27b, or whether it separates E_2 and perfect crystal (fig. 7.27c), in which case ΔE in equation 7.40 is now given by E_2. If this is the case, then the critical condition is likely to arise before the hemispherical configuration is reached. There is surprisingly little experimental evidence to resolve this

Fig. 7.28.   TEM micrograph of SIBM in copper deformed 14% in tension and
annealed 5 min at 234°C, (Bailey and Hirsch 1962).

point. Optical micrographs of Fe–Si (Dunn and Walter 1959) show some substructure in
the bulged region, and the transmission electron micrographs of Bailey and Hirsch
(1962) of copper, one of which is shown in figure 7.28, also show that the dislocation
density of the bulge, although lower than that of the parent grain, is significant, in
agreement with figure 7.27b. Simulations of SIBM using the vertex models
described in §16.2.4 show some such dragging of low angle boundaries behind the
migrating boundary, which is consistent with the results of Bailey and Hirsch
(Humphreys 1992b).

Bate and Hutchinson (1997) have shown that if SIBM proceeds as shown in figure
7.27b, as the bulge develops, the dislocation or boundary length attached to the bulging
boundary remains constant, whilst the boundary area is increased, and therefore the
restraining pressure due to the substructure acting on the concave side of the boundary
is reduced. They define the (constant) pressure on the convex side of the bulge as **P,** and
that on the opposite side as **P.f,** a fraction **f** of **P.** The critical length for bulging is then
found to be

$$R_{crit} = \frac{2\,\gamma_b}{\mathbf{P}\sqrt{1-\mathbf{f}}} \qquad\qquad (7.41)$$

compared to the Bailey and Hirsch value of equation 7.40, which can be written as

$$R_{crit} = \frac{2\,\gamma_b}{\mathbf{P}(1-\mathbf{f})} \qquad\qquad (7.42)$$

The implication of this analysis is that the critical bulge size is significantly reduced if the stored energy is large and ΔE is small $(f \rightarrow 1)$. As f increases, the difference between R_{crit} as given by equations 7.41 and 7.42 decreases.

7.6.2.2 Single subgrain SIBM

If SIBM occurs in a material with a well recovered subgrain structure, such as a low-solute aluminium alloy, it may originate at a single large subgrain as shown in figure 7.27d. In this situation there is no substructure drag, and equating the size of the critical bulge with the large subgrain, the critical subgrain radius is given by

$$R_{crit} = \frac{2\gamma_b}{P} \tag{7.43}$$

and taking P, the stored energy of an array of subgrains of radius R_i and boundary energy γ_1 as $3\gamma_1/2r_i$ (equation 2.7), we obtain, for growth of a bulge into grain 2, (c.f. Faivre and Doherty 1979)

$$R_{crit} = \frac{4\gamma_b R_2}{3\gamma_2} \tag{7.44}$$

where R_2 and γ_2 are the size and boundary energy of the subgrains in the upper grain 2.

For single-subgrain SIBM, there is no requirement for a stored energy difference in the two grains, merely that there is a subgrain of the critical size adjacent to the grain boundary. However, the critical subgrain size for SIBM decreases if there is a stored energy difference across the boundary. The viability of single subgrain SIBM is therefore dependent on the sizes, size distributions and boundary energies (or misorientation) of the subgrains in the two grains. In figure 7.29, we show the critical
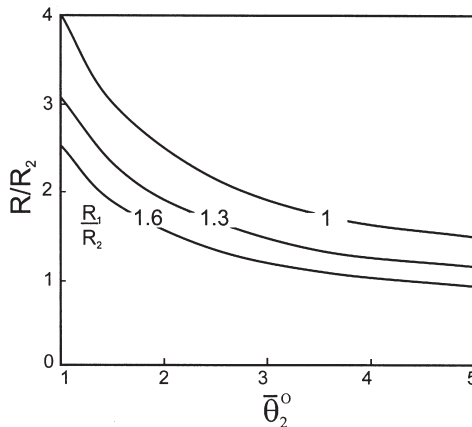

Fig. 7.29.   The critical size for a large subgrain in grain 1 to undergo SIBM, as a function of the mean subgrain misorientation in grain 2 and the relative sizes of the subgrains in the two grains, (Humphreys 1999a).

subgrain size for SIBM as a function of the subgrain sizes of the two grains and the mean subgrain misorientation in grain 2 (Humphreys 1999a).

For the case when the subgrain structures have the same mean size ($R_1/R_2 = 1$) it can be seen that when the mean misorientation is larger than $\sim 2°$ there is a reasonable probability of there being sufficiently large subgrains (R larger than ~ 2.5 times the mean subgrain size) on either or both sides of the high angle boundary to act as 'nuclei' for recrystallization. An energy difference across the boundary will of course make SIBM more viable and it can be seen from figure 7.29 that if $\bar{\theta}_2$ were 1° and $R_1 = 1.6R_2$ then a subgrain in grain 1 of size $2.5R_2$ (i.e. $1.6R_1$) would be capable of inducing SIBM.

The single subgrains large enough to induce SIBM can form during deformation (e.g. Humphreys and Hurley 2001). However, they might also arise from preferential recovery in the vicinity of a grain boundary, and Doherty and Cahn (1972) and Jones et al. (1979) have discussed how recovery by subgrain coalescence in the vicinity of a high angle boundary (§6.5.4) could initiate SIBM.

7.6.2.3 Multiple or single subgrain SIBM?

Multiple subgrain SIBM can occur under most conditions, because the critical nucleus size as given by equation 7.41 adjusts according to the conditions. However, if the stored energy difference (ΔE) between the grains becomes small, R_{crit} becomes improbably large. An important parameter is therefore the distance along the boundary over which any particular value of **f** is maintained. The maximum distance is the grain size, but it will usually be smaller. If we take 20 μm as a reasonable limit, then the conditions of **f** and θ_2 over which multiple subgrain SIBM can occur are as shown in figure 7.30.

The critical subgrain size for single subgrain SIBM is given by equation 7.44 and figure 7.29. The chances of there being a suitably large subgrain depend on the subgrain size distribution, and typically, subgrains up to around 3–4 times the mean are found. If we
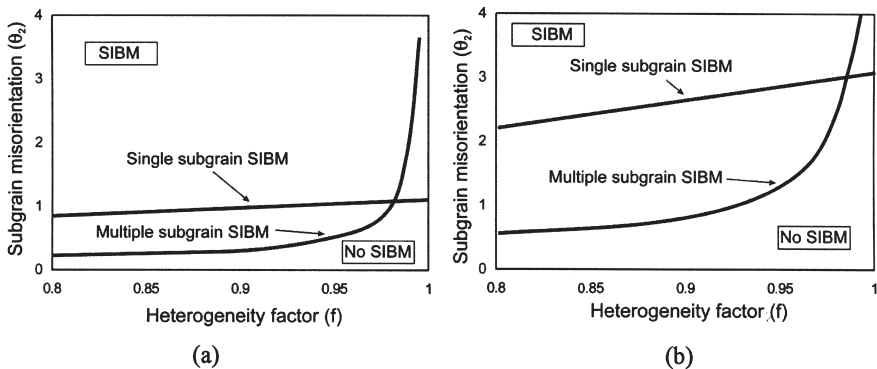

Fig. 7.30.   The conditions for SIBM from single or multiple subgrains as a function of the fractional difference (**f**) in stored energy of the two grains. In the upper region, both mechanisms can occur, but single subgrain SIBM is usually more rapid: (a) single phase alloy, (b) particle-containing alloy where $P_Z = 0.5P_D$.
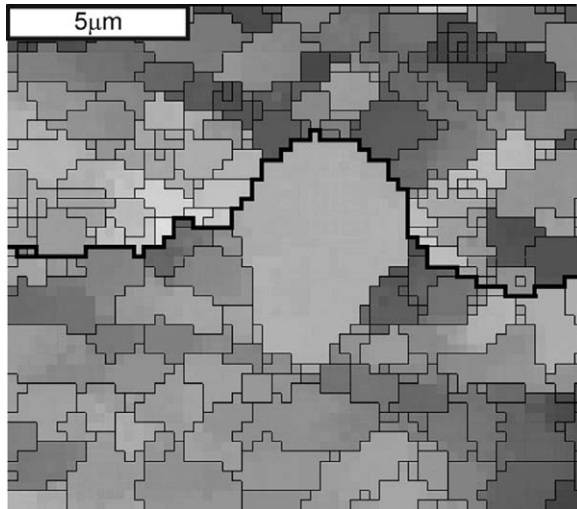
Fig. 7.31.   EBSD map showing SIBM in Al-0.1 wt%Mg, cold rolled 20% and annealed at 300°C. The colours depend on orientation, HAGBs are black and LAGBs are grey. No substructure is apparent in the recrystallized grain, (Courtesy of P.J. Hurley). (See colour plate section.)

take $4R_2$ as the maximum available size, then SIBM can occur if $\theta_2 > 1°$ when $R_1 = R_2$ (fig. 7.29). If we assume that changes in $\mathbf{f}$ are due to subgrain size differences alone, then the condition for single subgrain SIBM is as shown in figure 7.30a.

Calculations show that if both processes are viable, single subgrain SIBM is more rapid when the bulge sizes are close to critical, because of the lack of restraining pressure. Therefore we expect from figure 7.30a that single grain SIBM will dominate for substructures with misorientations larger than ~1°, and when the grains have similar stored energies. Investigations of SIBM in aluminium cold rolled ~20% (Humphreys and Hurley 2001) are consistent with single subgrain SIBM as there is no detectable substructure within the bulge as is shown in the EBSD map of figure 7.31. Multiple SIBM is to be expected for lower subgrain misorientations, and in materials in which poorly defined dislocation cells are formed, which is consistent with the earlier work of Bailey and Hirsch on copper. The presence of a dispersion of second-phase particles reduces the driving pressure and favours multiple subgrain SIBM, as shown in figure 7.30b and discussed in §9.4.1.

Despite the undoubted importance of SIBM in recrystallization, much additional work is required to clarify the details of the mechanism and the conditions under which it occurs.

7.6.3 The preformed nucleus model

In the process of strain induced grain boundary migration discussed above, the high angle grain boundary which is a prerequisite for recrystallization, was already in

existence. However, in many cases, recrystallization originates in a region of the material where there is no such boundary, and we need to consider how a nucleus may be formed in such circumstances.

The possibility that recrystallization might originate at crystallites present in the deformed material was first postulated by Burgers (1941). In his **block hypothesis,** the nuclei could be either crystallites which were highly strained, or ones which were relatively strain free. It is now established beyond reasonable doubt that recrystallization originates from **dislocation cells or subgrains which are present after deformation.** Although there are still uncertainties about how these pre-existing subgrains become nuclei, several points are now clear.

(i) The **orientation of the nucleus is present in the deformed structure.** There is no evidence that new orientations are formed during or after nucleation, except by twinning (§7.7). Although there are instances where the orientations of new grains appear to lie outside the spread of the deformation texture (Huang et al. 2000c), the most likely explanation for such observations is that the recrystallization has originated from very small regions which were not detected during texture analysis of the deformed material.

(ii) Nucleation occurs by the **growth of subgrains** by the mechanisms discussed in §6.5.3. All direct in-situ TEM annealing observations of recrystallization nucleation (Ray et al. 1975, Humphreys 1977, Bay and Hansen 1979) have shown the mechanism to be one low angle boundary **migration,** and there is no evidence that subgrain **coalescence** has a significant role. The in-situ HVEM experiments have shown that recovery in the vicinity of the nucleus is significantly faster than in the remainder of the material.

(iii) In order for a high angle grain boundary to be produced by this rapid recovery, there must be an **orientation gradient** present. This is shown schematically in figure 7.32 which shows two 1-dimensional subgrain structures with similar misorientations between the individual subgrains. Recovery by subgrain growth of the structure shown
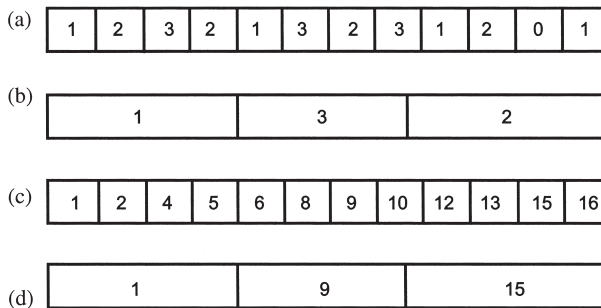

Fig. 7.32.   The effect of an orientation gradient on the recovery of a 1-D microstructure. The numbers represent the orientation of the subgrains with respect to the left edge of the microstructure: (a) there is no overall orientation gradient, (b) on annealing, no high angle boundary is formed, (c) there is an orientation gradient, (d) recovery leads to the formation of higher angle grain boundaries.

in 7.32a produces large subgrains but no high angle boundary (fig. 7.32b), whereas the same amount of recovery in the presence of an orientation gradient (fig. 7.32c) results in the formation of higher angle grain boundaries (fig. 7.32d). This important point was first clearly stated by Dillamore et al. (1972). It should be noted that any region with a large orientation gradient will **always** have a high stored energy because of the geometrically necessary dislocations or low angle grain boundaries, which are needed to accommodate the misorientation. As discussed in §6.5.3.4, theory predicts that recovery will be most rapid in regions of large orientation gradient.

Nucleation of recrystallization in such a situation can therefore be considered as no more than discontinuous subgrain growth at sites of high strain energy and orientation gradient.

The **site** of the nucleus is very important in determining its viability, and it is found that the general mechanism discussed above can occur at a variety of sites.

7.6.4 Nucleation sites

Recrystallization will originate at inhomogeneities in the deformed microstructure. These may be associated with pre-existing microstructural features such as second-phase particles (§2.9.4) or grain boundaries, or may be inhomogeneities induced by the deformation, as discussed in chapter 2. As the orientation of a recrystallized grain will depend upon the recrystallization site, the types of site which operate may have a strong effect on the **recrystallization texture** as discussed in chapter 12.

7.6.4.1 Grain boundaries
Nucleation in the vicinity of prior grain boundaries, of new grains of orientations which are not close to those of the parent grains, has been frequently reported (e.g. Beck and Sperry 1950), and is more frequent at larger strains. Some evidence of the operation of such a mechanism has been obtained by Hutchinson (1989) in iron bicrystals in which the new grains were misoriented by 30° from the parent grains, and in aluminium bicrystals (Driver et al. 2000). Little is known about this type of recrystallization or about the orientations of the resulting grains. However, it is known that grain boundaries give rise to inhomogeneity of slip (Ashby 1970, Leffers 1981), and that different combinations of slip systems may operate near grain boundaries (§3.7.1), thereby giving rise to local misorientations in a manner which is probably similar in principle to that which occurs near large second-phase particles (§2.9.4). It is therefore likely that recrystallization originates in the regions of large orientation gradient which will be present near some grain boundaries or triple junctions. Whether or not there is a real distinction between this mechanism and that of SIBM has not been clearly established.

7.6.4.2 Transition bands
A transition band separates parts of a grain which have split during deformation into regions of different orientation (§2.7.3). A transition band is therefore a region of large orientation gradient which is an ideal site for recrystallization. Recrystallization at transition bands was first reported in iron by Hu (1963) and Walter and Koch (1963). The crystallographic orientations developed in transition bands are a direct consequence
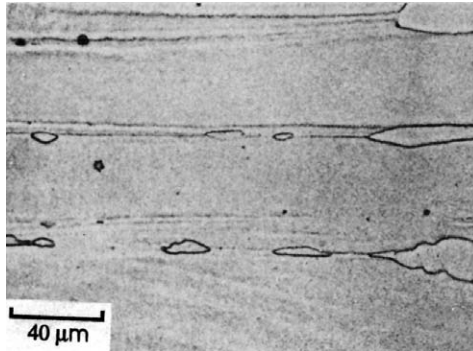
Fig. 7.33.   Optical micrograph showing recrystallization at transition bands in a
silicon–iron crystal, (Hu 1963).

of the slip processes and the strain path and therefore the recrystallized grains tend to
have preferred orientations. Because of its importance in determining the recrystalliza-
tion texture of metals (chapter 12) there have been many extensive studies of this
mechanism including those of Bellier and Doherty (1977) and Hjelen et al. (1991) on
aluminium, Inokuti and Doherty (1978) on iron and Ridha and Hutchinson (1982) on
copper. An early example of nucleation at a transition band in iron, from the classic
work of Hu is shown in figure 7.33.

An example of recrystallization in a transition band in a cube-oriented crystal of
aluminium, deformed at high temperature, from the work of Huang et al. (2000b) is
shown in the EBSD map of figure 7.34. The crystal has deformed inhomogeneously as
shown in figure 7.34a and the regions within 15° of the original cube orientation are
shaded dark. There is a large orientation gradient across the band (figure 7.34b), and on
annealing, subgrain growth in this region is rapid (see §6.5.3.6 and figure 6.22), resulting
in the accumulation of a large misorientation, so that a high angle boundary is produced
after a small amount of growth, and recrystallization is then initiated.

7.6.4.1 Shear bands

Shear bands in rolled metals are thin regions of highly strained material typically
oriented at ~35° to the rolling plane. They are a result of strain heterogeneity due to
instability during rolling and their formation is strongly dependent on the deformation
conditions as well as the composition, texture and microstructure of the material (§2.8).
Nucleation of recrystallization at shear bands has been observed in many metals
including copper and its alloys (Adcock 1922, Duggan et al. 1978a, Ridha and
Hutchinson 1982, Haratani et al. 1984, Paul et al. 2002), aluminium (Hjelen et al. 1991)
and steels (Ushioda et al. 1981). An early micrograph showing profuse nucleation at
shear bands in copper is shown in figure 7.35.

Details of the mechanism of nucleation at shear bands are not known, and the
orientations of the grains so formed appear to be very case dependent (Nes and
Hutchinson 1989). For example in α-brass (Duggan et al. 1978a) the orientations of the
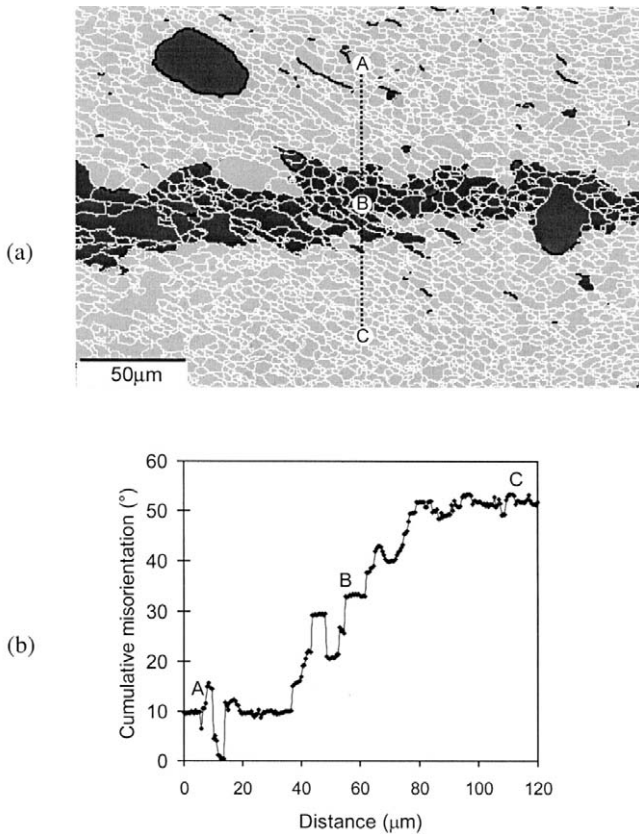grains were widely scattered, but in aluminium (Hjelen et al. 1991), the grains were of

Fig. 7.34.   EBSD of a hot-deformed and annealed aluminium crystal of cube orientation, showing recrystallization originating in a band of large orientation gradient: (a) map in which the regions close to the cube orientation are shaded dark. High angle boundaries are black and low angle boundaries are white, (b) the change in misorientation along the marked line A-B-C, (Huang et al. 2000b).

orientations close to the **S** {123} < 634 > texture component. The orientations of the grains formed in shear bands, and their influence on the recrystallization texture are further discussed in §12.2.1.2.

7.7 ANNEALING TWINS

7.7.1 Introduction

During the recrystallization of certain materials, particularly the face centred cubic metals of intermediate or low stacking fault energy such as copper and its alloys and
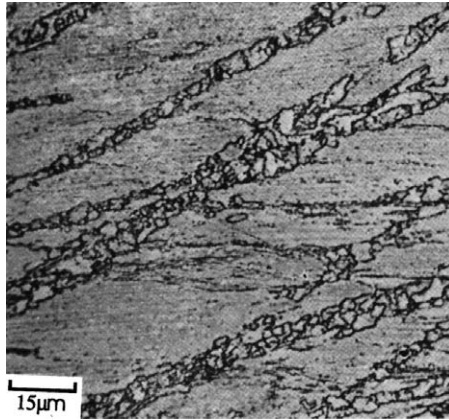
Fig. 7.35.   Optical micrograph showing recrystallization occurring at shear bands in copper, (Adcock 1922).
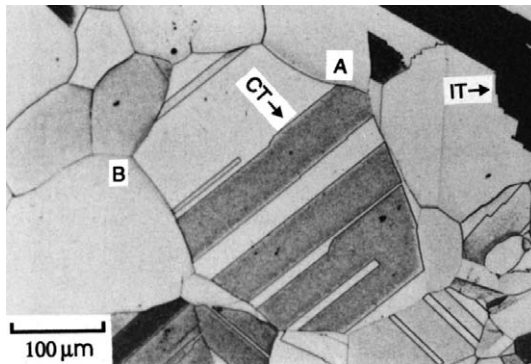

Fig. 7.36.   Annealing twins in annealed 70:30 brass. Some coherent (CT) and incoherent (IT) twin boundaries are marked, (courtesy of M. Ferry).

austenitic stainless steels, annealing twins are formed as seen in figure 7.2. Such twins are also found in many intermetallic compounds, ceramics and minerals. These twins take the form of parallel sided lamellae as shown in figure 7.36. In fcc metals the lamellae are bounded by {111} planes or **coherent twin boundaries (CT)** and at their ends or at steps, by **incoherent twin boundaries (IT)** as shown in figure 7.36. The nature of these boundaries is discussed in more detail in §4.4. Twins may form during recovery, primary recrystallization or during grain growth following recrystallization, and their formation during the recrystallization of copper may be seen in the in-situ annealing sequence of figure 7.2. It should be noted that twin formation does not only occur during annealing, but may also occur during solid state phase transformations (Basson et al. 2000) or during solidification (Han et al. 2001), and of course during plastic deformation, although these types of twinning will not be considered further.

There has been recent interest in improving the properties of alloys by controlling the grain boundary character **(Grain Boundary Engineering),** and maximising the number of low Σ boundaries such as $\Sigma 3$ twins through thermomechanical processing, and this is further discussed in §11.3.2.3.

7.7.2 Mechanisms of twin formation

Although twins have been extensively studied, the atomistic mechanism of their formation remains unclear. The growth of twins may take place in two configurations as shown in figure 7.37. In figure 7.37a the growth direction is perpendicular to the coherent twin boundary and in figure 7.37b it is parallel.

7.7.2.1 Twinning by growth faulting

Gleiter (1969c, 1980) proposed that twinning occurred by the movement of ledges on the coherent twin boundary. As the twin propagates by addition of the close packed planes in a sequence such as ABCABC, the start or finish of the twin lamella requires only the nucleation and propagation of a ledge with a low energy growth fault such as to change the sequence e.g.

ABCABC|BACBACBA|BCABC.

Whilst this mechanism is capable of explaining twins propagating as shown in figure 7.37a, it is not consistent with the configuration of figure 7.37b.

7.7.2.2 Twinning by boundary dissociation

Goodhew (1979) found evidence for twin formation by boundary dissociation in gold. He identified the following dissociations:

$$\Sigma 9 \rightarrow \Sigma 3 + \Sigma 3$$
$$\Sigma 11 \rightarrow \Sigma 3 + \Sigma 33$$
$$\Sigma 33 \rightarrow \Sigma 3 + \Sigma 11$$
$$\Sigma 99 \rightarrow \Sigma 3 + \Sigma 33$$

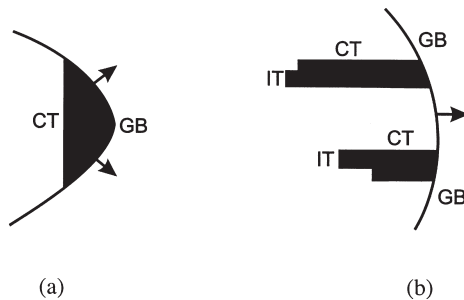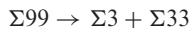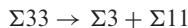(a)   (b)

Fig. 7.37.   Possible orientations of twins during recrystallization: (a) the coherent twin (CT) boundary lies parallel to the recrystallization front, (b) the CT boundary is perpendicular to the recrystallization front, (after Goodhew 1979).
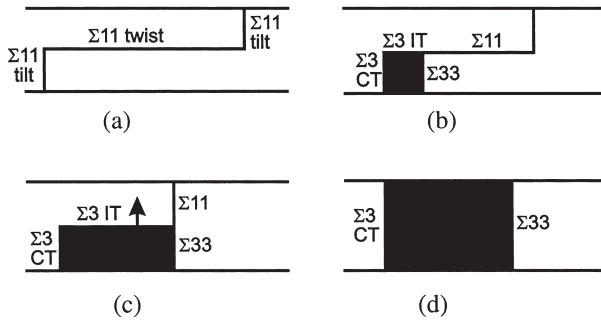
Fig. 7.38.   Possible mechanism for the dissociation of a Σ11 boundary. During tilt boundary migration (a), one of the tilt boundaries dissociates (b), leaving a twin behind. The remaining Σ11 twist boundary is then eliminated (c), and the incoherent twin boundary (IT) then migrates to remove the remaining Σ11 boundary (d), (Goodhew 1979).

In all these cases a decrease in energy results (Hasson and Goux 1971), and a possible mechanism for this is shown schematically in figure 7.38.

It has been suggested that this type of boundary dissociation could occur by the emission of grain boundary dislocations, and variants of this type of mechanism have been suggested by Meyers and Murr (1978) and Grovenor et al. (1980).

7.7.3 Twin formation during recovery

Huber and Hatherly (1979, 1980) reported the formation of **recovery twins** in shear bands, during the annealing of deformed 70:30 brass at ~250°C, some 30°C below the recrystallization temperature. They were ~250 nm long and ~2–10 nm wide. Only one set of twins developed in a particular region, and these were always associated with local orientations of the form {110}<112>. The twins increased in number and width as annealing continued and there was a gradual loss of dislocations from the regions where they occurred (fig. 7.39). This loss appeared to correspond to the beginning of recrystallization, but it is significant that there was no clearly defined boundary around the developing nucleus.

7.7.4 Twin formation during recrystallization

7.7.4.1 The role of twinning
As twinning produces new orientations that were not present in the deformed microstructure, twinning may play an important part in the development of annealing textures (§12.3.5). An extensive research programme by Haasen and colleagues at Göttingen (e.g. Berger et al. 1988) has shown that multiple twinning in the early stages of recrystallization may be important in determining grain orientations in copper alloys. Their conclusion, based on in-situ high voltage electron microscopy annealing
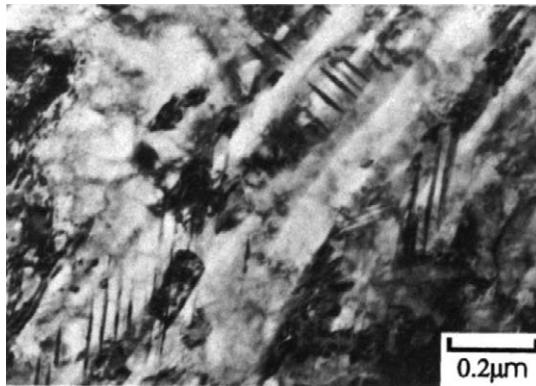
Fig. 7.39.   Recovery twins in 85:15 α-brass, deformed in torsion and annealed at
240°C, (Huber and Hatherly 1979).

experiments (Berger et al. 1983) that twinning plays an important role in the
recrystallization of aluminium is controversial. Twins are rarely observed in bulk
samples of aluminium and it is likely that twin formation in this material is influenced
by the free surfaces as discussed in §7.7.4.3.

7.7.4.2 Twin selection principles

If multiple twinning were to occur in a random manner then a random texture would
result (§12.3.5). However, the recrystallization texture of heavily deformed copper (fig.
12.1) is a very strong cube texture with little contribution from twins. It is known (e.g.
Hatherly et al. 1984) that only a few of the possible twin variants are formed, and
therefore twinning during recrystallization cannot occur randomly and some selection
principles must apply. Wilbrandt (1988) has reviewed these in detail and concluded that
no single principle is capable of explaining all experimental observations. However, the
following three factors have been shown to be important.

- **Boundary energy**

There is a large body of evidence which suggests that the lowering of grain boundary
energy is a very important factor in determining the twin event and provides stability of
the grain against further twinning. The work of Goodhew (1979) discussed above, and
of the Göttingen group (Berger et al. 1988) has provided good evidence in support of
this principle.

- **Grain boundary mobility**

The possibility that twinning occurs in a manner such as to provide a more mobile
boundary has also been considered. For example during dynamic recrystallization of
copper and silver single crystals (Gottstein et al. 1976, Gottstein 1984) (see §13.3.6), it
was found that multiple twinning occurred until a fast growing grain orientation was
formed. If this were the overriding factor however, we might expect twin chains to result
in progressively more mobile boundaries, whereas it is known that twinning sometimes
results in very immobile boundaries (Berger et al. 1988).

● **The role of the dislocation arrangement**

Evidence that twinning is affected by the dislocation structure has been presented by Form et al. (1980) who found that the twin density increased with the dislocation density. Rae et al. (1981) and Rae and Smith (1981) found that both dislocation structure and the grain boundary orientation were important in determining the ease of twinning.

7.7.4.3 Twinning and interfaces

In-situ annealing experiments on aluminium in the SEM (Humphreys and Ferry 1996), and comparison with the bulk microstructures, have shown that twin formation during recrystallization is much more prolific at a free surface than in the sample interior. It was also found that in two-phase aluminium alloys, twins were frequently associated with large second-phase particles. Although the reasons for this are not entirely clear, it is likely that the presence of a high energy surface or interface plays a significant role, as it does in twin formation during grain growth as discussed below. Significant numbers of twins may also be formed during the recrystallization of aluminium alloys containing dispersions of small second-phase particles (Higginson et al. 1995, Lillywhite et al. 2000), although the reasons are not clear.

7.7.5 Twin formation during grain growth

The early work on twin formation was mainly concerned with their formation during grain growth (Burke 1950, Fullman and Fisher 1951). The postulated mechanism of twinning, which is based on an energy criterion is shown in figure 7.40.

In figure 7.40a, grain growth is occurring such that the triple point between grains A, B and C is moving vertically. As growth proceeds, it is assumed that a growth fault may occur at some point leading to the formation of a grain (T) which is twinned with respect to grain A. If the relative orientations of the grains are such that the energy of the boundary AT is lower than that of AC then, because the energy of the coherent twin boundary AT is very low (table 4.2), there may be a reduction in total boundary energy
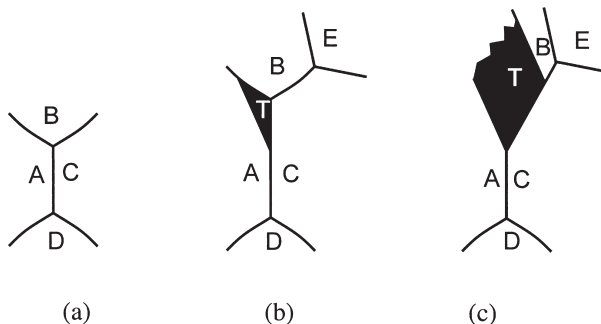

Fig. 7.40.   Mechanism for twin formation during grain growth following recrystallization.

despite the extra boundary area created, and therefore the twin configuration will be stable and grow. This condition, in two dimensions, is:

$$\gamma_{AT} L_{13} + \gamma_{TC} L_{23} + \gamma_{TB} L_{12} < \gamma_{AC} L_{23} + \gamma_{AB} L_{12} \qquad (7.45)$$

where γ_{ij} is the energy of the boundary between grains i and j and L_{xy} is the distance between points x and y.

The growth will be terminated if the triple point ABC reacts with another triple point such as BCE, resulting in a grain configuration with a less favourable energy balance (fig. 7.40c). On such a model, the number of twin lamellae should be proportional to the number of triple point interactions, and evidence for this was found by Hu and Smith (1956). The actual atomistic mechanism of twin formation during grain growth is likely to be similar to the mechanisms discussed above for twin formation during recrystallization.
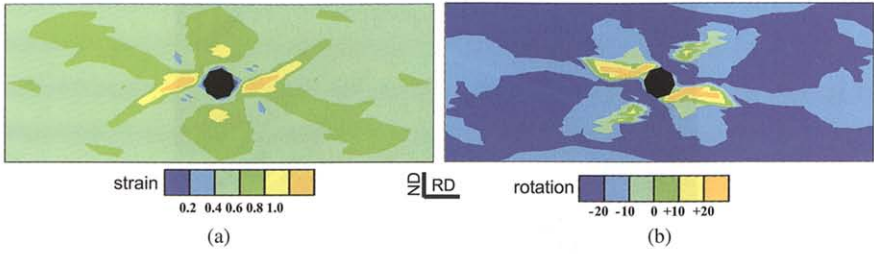
strain ◼◼◼◼◼◼
0.2 0.4 0.6 0.8 1.0

ND RD

rotation ◼◼◼◼◼◼
-20 -10 0 +10 +20

(a)   (b)
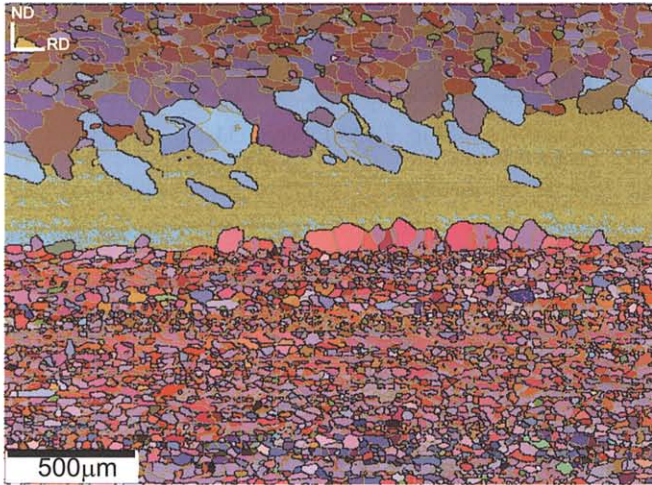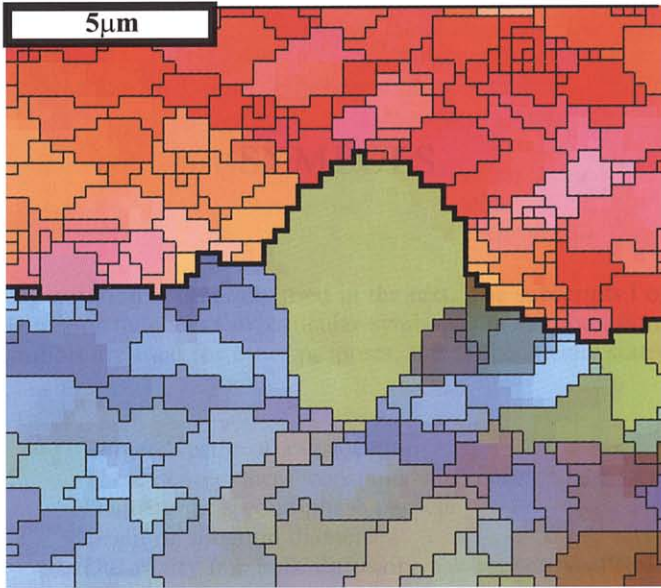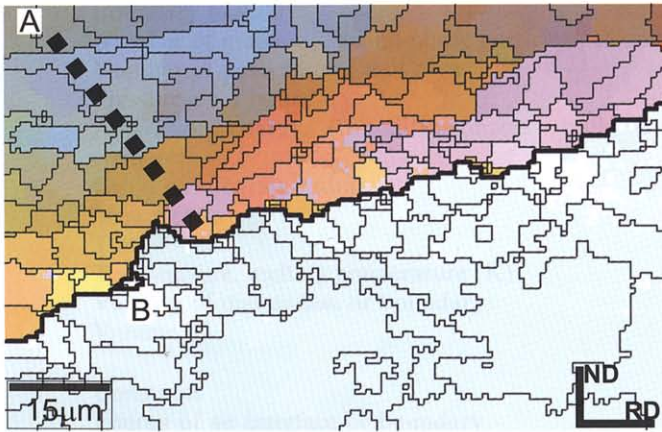
Fig. 2.39. See p. 64.

ND
RD

500μm

Fig. 7.15. See p. 240.

Fig. 7.31. See p. 257.

Fig. 13.22(a). See p. 440.